J. Cosmet. Sci., **67,** 121–159 (May/June 2016)

Probing the textures of composite skin care formulations using large amplitude oscillatory shear

TIMOTHY GILLECE, ROGER L. MCMULLEN, HANI FARES, LARRY SENAK, SEHER OZKAN, and LINDA FOLTIS, *Ashland, Inc., Bridgewater, NJ 08807.*

Accepted for publication May 30, 2016.

Synopsis

Identifying meaningful and measurable rheological parameters that shadow the dynamic shear stresses sustained in the initial application and subsequent spreading of structured cosmetic formulations onto the skin is quite challenging. When applied to non-Newtonian soft solids, traditional oscillatory rheological testing tends to best correlate with the "at-rest" state, or, more fundamentally, with the initial and thermodynamically reversible perturbations in the physiochemical networking that binds components of the amalgamated microstructure. In addition, after yielding, as an applied film is further thinned while spreading on the skin surface, shear rates during flow processes may rapidly and dynamically increase to 10^4 s^{-1}, which is a magnitude that is not practically simulated with a standard rotational rheometer. Realistically speaking, it is rare that a single rheological measurement or resultant parameter predicts the sensorial appeal of a complex fluid during the entire scope of a spreading process.

Large amplitude oscillatory shear (LAOS) methodology is an augmentation of standard oscillatory rheology, or small amplitude oscillatory shear (SAOS), and delivers a means to dynamically probe the deforming microstructure of a soft solid as it rheologically transitioned from a viscoplastic material to a structured fluid. LAOS rheology was performed on four different prototypes having different skincare textures to produce Bowditch–Lissajous plots (henceforth truncated to *Lissajous* in the remainder of the document) for subsequent association with previously measured sensorial properties. Insights into the shapes of the curves and their relation to paralleled sensorial analyses are primarily based on the performance of the composite prototypes rather than speculating on the individual contribution of each constituent to the dynamics of the adapting microstructure. Therefore, transitions in the Lissajous trajectories may be used to visually describe changes in the bulk rheology as the physical components of the local viscoelastic environment are controllably sheared.

In this work, Lissajous profiles are amassed with smooth and rough surfaces data utilizing standard rheological techniques, including oscillatory SAOS, stress ramps, Brookfield viscometry, and the manifestation of interfacial or complex flow properties, such as wall-slip and shear-banding phenomena. Practical influences on the human stratum corneum, including thermal softening and electrostatic shielding, are also considered. Additionally, outcomes from texture profile analysis are reported and contrasted with the accompanying results. Ultimately, the objective is to make meaningful connections between trends in Lissajous trajectories and paralleled sensorial analyses conducted by a trained expert panel. For the reader, a basic level of rheological knowledge is assumed.

Address all correspondence to rmcmullen@ashland.com.

INTRODUCTION

The tactile perception of substances is a personal physiological experience that varies from observer to observer and is dependent on the local sensory/nerve structures of the individual (1). Moreover, other perceptions, such as vision and smell or wishful thinking, may subconsciously bias the tactile experience. For this reason, panels of experts are often used to objectify tactile observations. Even the most expert panelist, however, cannot cleanly sort out the rheological contributions to the tactile experience. How these experiences add up to the observer's impressions will vary between panelists no matter what precautions are taken to ensure objectivity. When rheological techniques are applied to complex fluids, they most often provide a collection of individual parameters that feed into discerning neat material properties, rather than expressing the full spectrum of physiological challenges from the *in vivo* tactile experience. For this reason, rheological outcomes are often not intuitive, or do not fully describe palpable differences in the sensorial experience. We propose to leverage specific rheological techniques that close the gap in understanding measurable contributions influencing textural properties, while implicitly arguing that perhaps a less complex, "one-pot" visualization of an array of rheological properties more succinctly elucidates distinctions in the complex textural properties of substances.

Successfully correlating textural properties with rheological properties involves a thorough understanding of the strengths and weaknesses of the measurement, as well as an appreciation for the tactile perception limits and complexity of the human somatosensory system—where signals from pressure, skin stretch, vibration, itch, and/or temperature are translated from touch via specialized sensory organs in the skin to the spinal cord and, finally, to the brain for processing (2). Further, and to complicate matters, applying certain topical products to the skin may alter specific surface properties, thereby altering the mechanical stimulation of the skin (3). Although the biology of the individual is essentially fixed, training the human to duplicate the restricted motions of a rheometer or texture analyzer, or configuring the instrumentation to mimic the methodology of the sensorial challenge, is a valid option. Even more complex, each person's biology and interpretation of perception is unique, leading to a natural bias in the panel data. Further, the unmistakable reality is that not all instrumental outputs relate to discernible sensorial properties; and, understandably, no single result resolutely defines the complex gamut of end-use textural appeal. Malcolm Bourne summarizes this emblematically by noting that there are many measurable wavelengths of electromagnetic radiation, but only select wavelengths between 400 and 700 nm (i.e., visible light) are perceptible; basically, many instrumental techniques detect physical properties in materials that are not necessarily discernible by the somatic senses (4).

Although daunting, many researchers have attempted sensorial correlations with the ambition of developing predictive measurement models to mitigate the potential subjectivity, sizeable cost, and time demands of using trained professional panelists for sizeable sensorial studies on cosmetic formulations (5–8). Many have focused on using parameters from flow models, such as the power law, or the yield stress and consistency parameters of the viscoplastic Herschel–Bulkley or Casson relationships (9). Some have focused on SAOS parameters to gauge the initial spreadability, cushion, or body of a structured system, while the 2010 work by Greenaway found the correlation of firmness, thickness, and the resistance and difficulty of spreading with trends in the elastic modulus at high strain (10); others have focused on combining rheological and texture analyses to make paral-

lels (8,11). Prior work also included sensorial correlations with discrete Fourier transform (DFT) and Chebyshev polynomials derived from LAOS experiments; correlations included initial spreading, pick up, and cushion for a series of anionic hydrogels (12).

In the current study, SAOS and flow methodologies were performed on texture prototypes to better understand the impact of viscosity, frequency, yield stress, thixotropy, and nonlaminar flow on the shapes of the Lissajous plots; however, the principal objective of this work was to investigate the parallels between sensorial texture ratings and the trajectories of the Lissajous loops as a sample is deformed rotationally from the linear viscoelastic region (LVR) to large strains and high oscillatory shear rates using dynamic strain sweep experiments. Within the LVR, the loop trajectory mostly represents the at-rest state, whereas at very high strains, the Lissajous figures present a transition to a flowing structured fluid. Manipulating the resultant nonlinear Lissajous data enables decomposition of the data into additional descriptive parameters. For example, performing DFT on the data subsequently enables conversion of the time-based (or temporal) stress response to the frequency domain. The population of each harmonic term in the frequency distribution is, hence, derived from the nonlinear stress-wave shape. The insights provided by this decomposition are reflected in the introduction of additional Lissajous curves that track the trajectory of the elastic component of stress as a function of strain or shear rate. Thus, a formulator may better understand how the component of stored energy (or the energetic wish to fight back against the will of the forced rotation) influences the magnitude of the total stress and the quality of the sensorial experience.

SAOS TO LAOS AND THE RESULTING LISSAJOUS PLOTS

Traditional dynamic oscillatory shear testing (SAOS) is conventionally applied to materials to determine a material's at-rest microstructural properties, such as the magnitudes of the frequency-dependent elastic modulus [$G'(\omega)$], loss modulus [$G''(\omega)$], complex viscosity [$\eta^*(\omega)$], and tan delta [$\tan \delta(\omega)$]. SAOS properties are studied in the LVR, where the driving forces that restore the structure stem from thermal energy (i.e., Brownian motion). In traditional oscillatory testing using a strain-controlled rheometer, a sinusoidal shearing strain is applied to the sample, and the sinusoidal stress response is simultaneously measured with the torque transducer (see wave interaction in Figure 1). Elastic samples exhibit no shift in phase (δ) between the applied strain and the measured stress response, whereas viscous samples have a phase shift of 90°. Viscoelastic materials, which comprise both viscous and elastic properties, exhibit phase shifts ranging from 0° to 90° between the absolute value of the stress (σ) and strain (γ) maxima. Imagine 45°–90° to be a viscoelastic liquid ($G' < G''$), where 45° is a 1:1 balance of elastic and viscous stress ($G' = G''$), and 0°–45° to be a viscoelastic solid ($G' > G''$). For clarity, note that the term "sinusoidal" refers to the shape of the wave that is obtained by plotting strain as a function of time (t) in the following parametric equation:

$$\gamma(t) = \gamma_0 \sin(\omega t) \qquad (1),$$

where ω is the angular frequency (in rad/s) of the applied strain. Figure 1 implies the interplay between the applied strain, which is imparted by an oscillating motor, and the

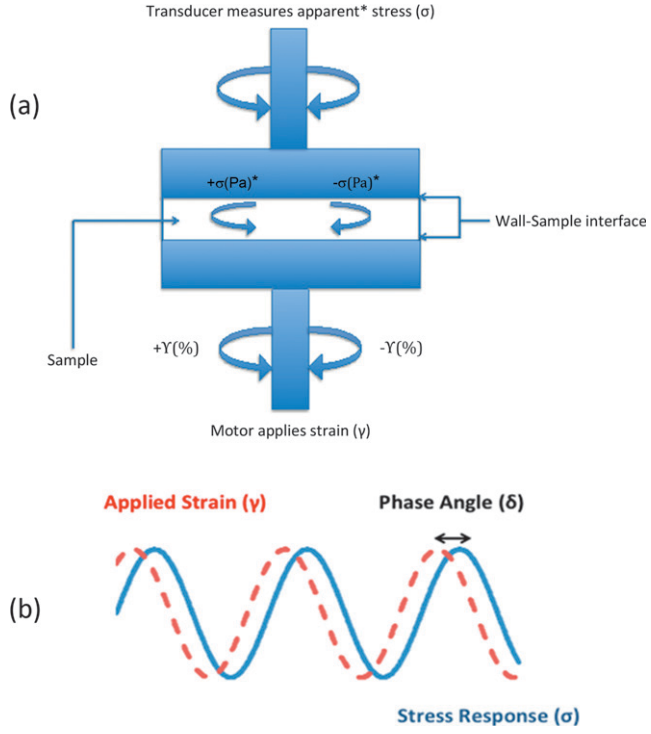

Figure 1. (A) The position of the sample within the parallel plates. An ARES G2 rheometer has a separate motor from the transducer design to mitigate the complexities of inertia. (B) The motor exerts a deformation on the sample and the torque is converted to the stress response. The phase lag relates to properties of viscoelasticity.

translation of these stresses to the sample, which are subsequently transferred to the force transducer of the rheometer. Note that the torque imparted to the transducer through the sample junction clearly depends on the microstructure of the sample as well as its interfacial and tribological association with the composition of the plates (e.g., stainless steel, acrylic) that are affixed to the transducer and motor. Interfacial factors, such as wall slip, confound the meaning of the measurements (13,14). Wall slip occurs when there is slippage of the sample at the interface with the geometry of the rheometer—leading to erroneous results or, more accurately, to a flawed interpretation of microstructural strength. Normally, using rheometer geometries with roughened surfaces can circumvent slip phenomena.

Unfortunately, beyond the constraints of the LVR, the stress response wave will no longer appear sinusoidal, and the traditional mathematical SAOS functions, which are based on the premise that both the applied and response waves are sinusoidal, are subsequently tainted by the addition of higher frequency wave harmonics (i.e., anharmonic stress response). Consequently, as the deformation amplitude traverses further from the LVR, the shape of the stress response wave and the physical meaning of the SAOS parameters, which are primarily used to gauge the physically reversible perturbations within a microstructure, become progressively more meaningless. That is, since only the fundamental harmonic of the stress response is used to calculate, e.g., the elastic modulus, the calculation may become increasingly inexact as other higher harmonics become involved

in storing elastic energy. Moreover, the primary motives for applying nondestructive forces and deformations in SAOS are to study time- or temperature-dependent changes in the material; and, although the Hookean domain provides a mechanical fingerprint of the microstructure, studying the rheological properties under larger, anharmonic deformations (i.e., LAOS) correlates more suitably to the end use of structured viscoelastic fluids, including properties such as breakdown and texture (15).

The introduction of LAOS, FT-rheology and the utilization of orthogonal Chebyshev polynomials potentially address and augment standard SAOS theory by introducing additional parameters that have a physical meaning (16). The Lissajous plots, which are essentially a visualization of the mathematical interference between the applied strain wave and the stress wave response, give visual insights into a material's mechanical response to applied temperature and shear. Lissajous profiles are influenced by the frequency, amplitude, and initial phase difference (see phase angle in Figure 1) between the superposed waves. In the LVR, where the waves are sinusoidal and essentially of equal frequency, and where there is little contribution from higher frequency harmonics, a plot of oscillatory stress versus oscillatory strain for a highly elastic sample appears in the Lissajous plot as a line or a very thin ellipse with a positive slope (where the minor axis of the ellipse centers above and below the origin). In contrast, for a completely viscous sample, the shape of the stress versus strain Lissajous curve is circular (see Figure 2). Ideally, unless there are issues with the sample or methodology, the loops are symmetrical around strain = 0, or shear rate = 0, because the positive Cartesian trajectory of the loop represents positive angular displacement, whereas the negative trajectory of the loop reflects the stress response to strain applied in the reverse angular direction. The inverse relationship between the stress versus strain and stress versus shear rate plots is a result of the shear rate ($\dot{\gamma}$) being the time derivative of strain [i.e., $\gamma(t) = \gamma_0 \sin(\omega t)$ and $\dot{\gamma} = d\gamma/dt = \gamma_0 \omega \cos(\omega t)$, where the cosine and sine trigonometric functions naturally differ in phase by $\pi/2$ rad or 90°]. Consequently, in perfect Newtonian flow, the stress is proportional to

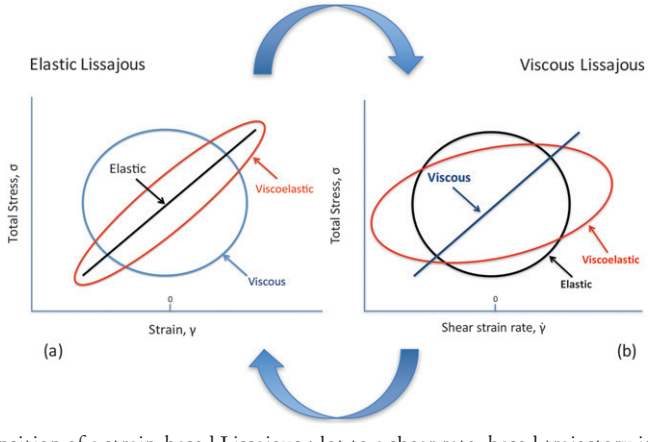

Figure 2. The transition of a strain-based Lissajous plot to a shear rate–based trajectory influences the visual meaning of the diagram. If a sample is elastic, a plot of stress versus strain results in a line (A); however, if the same sample is plotted versus shear rate, a circular trajectory will emerge (B). A viscoelastic sample will appear as an ellipse as it contains both elastic and viscous character. Note: In the elastic Lissajous plot, the slope of the semimajor axis of the ellipse is the complex modulus (G^*), and the area is proportional to the average energy dissipated within the cycle (i.e., G'').

the shear strain rate. In summary, because the strain rate is the time derivative of strain, a line is produced in a stress versus strain Lissajous plot for an elastic sample (elastic Lissajous plot, see Figure 2A), and a line is the result of a stress versus shear rate Lissajous plot for a perfectly viscous material (viscous Lissajous plot, see Figure 2B).

Outside the LVR, phase shifts and/or increases in contributions from higher stress harmonics (as evidenced by a distortion in the sinusoidal shape of the measured stress wave) produce distorted-elliptical loop shapes within the many-looped Lissajous plot that vary with the changing strain steps within the dynamic strain sweep experiment. In other words, a soft, yet structured, sample may appear elastic within its LVR, but may then demonstrate changes in structure as a function of increasing strain such that its last loop will suggest a completely viscous response. Additional trends include a clockwise "tilt" in the loops as a function of increasing strain, which is an indication of softening of the bulk material; furthermore, deviations from ellipticity, especially with upward/downward pointing tips, reflect intracycle strain stiffening (16). Many materials become stiffer when a stress is applied—where intracycle strain stiffening conveys a material's local, nonlinear elastic response within the span of a single oscillation step.

Finally, to get a better understanding of the instrumentation and variation in the transient shear rates encountered in a dynamic strain sweep step, if the absolute value of the stress response is considered as a function of strain, the maximum stress typically occurs at the maximum controlled strain (see Figure 2A), and the lowest measured stress is produced at 0% strain. Now, switching to the shear rate plot (see Figure 2B), the shear stress peaks at the maximum shear rate—or, more simply, at the highest angular velocity. Note the symmetry of the Lissajous loops around zero shear rate, where the stress maxima (think absolute value) are encountered at both the negative and positive shear rate boundaries for each oscillation step (Figures 1B and 2). To add more complexity to the mental picture, the maximum shear rate occurs at 0% strain, as the motor driving the sample deformation moves midway between the strain maxima (imagine a swinging pendulum at the bottom of its arc). Additionally, the angular velocity is zero at the maximum strain because the motor driving the sample physically stops for a moment to shift directions (imagine a swinging pendulum coming to a temporary halt at the top of its arc); hence, as the motor twists and turns during a single oscillation step, there are subtle differences in motor velocity that translate into variations in oscillatory shear rate.

DFT AND CHEBYSHEV POLYNOMIALS

FT-rheology involves decomposition of the raw stress response into its individual harmonics (Eq. 2).

$$\sigma(\omega,\gamma) = \sigma_1 \sin(\omega_1 t + \varphi_1) + \sigma_3 \sin(3\omega_1 t + \varphi_3) + \sigma_5 \sin(5\omega_1 t + \varphi_5) + \ldots \quad (2),$$

where σ, γ, ω, and t have already been defined as the stress, strain, angular frequency, and time, respectively, and φ_i corresponds to the phase difference between the applied strain and the harmonic components of the stress response. In a nutshell, equation (2) suggests that the nonsinusoidal response in LAOS is best contained and described by a series of parametric terms in which the frequency contributions from the higher harmonics

are proportioned with the fundamental harmonic to best fit the shape of the deformed wave. The odd harmonics are then extracted, and the resultant frequency data are subsequently recasted into nonlinear parameters—instead of just G', G'', tan δ, etc.—as a function of the originally applied strain magnitude (or shear rate). The nonlinear materials properties include nonlinear elastic moduli (G'_L and G'_M), the strain-stiffening ratio (S), and the shear-thickening ratio (T). G'_L is a measure of the elasticity at large strains, whereas G'_M is the residual elasticity of a material as it flows at the highest oscillatory shear rate. Consequently, the nonlinear coefficients facilitate a more complete description of the local or instantaneous stress response during the sweep of a single oscillation, whereas traditional rheology focuses on the average stress response to the deformation. As sensorial processes are dynamic, it can be argued that panelists sense the most extreme relative rheological transitions, and that an understanding of the divergence in nonlinear parameters is critical to successfully garnering correlations. Finally, from the isolated odd harmonics, the total stress (σ) can be subsequently recasted as temporal data and separated into its elastic (σ') and viscous (σ") components.

Using an application of orthogonal Chebyshev polynomials, Ewoldt and McKinley provide a means for the physical interpretation of a nonlinear stress response, with a means to methodically characterize nonlinear elastic (e_n) and viscous (v_n) parameters (where n = 1st, 2nd, 3rd, etc., harmonic intensities). The result nets the Chebyshev intracycle, or local, viscous, and elastic coefficients, where $e_3 = 0$ and $v_3 = 0$ in the LVR; further $e_3 < 0$ implies strain softening, $e_3 > 0$ indicates strain stiffening, $v_3 < 1$ describes shear thinning, and $v_3 > 0$ corresponds to shear thickening (16). In addition, the coefficients also enable a direct mathematical connection between the Chebyshev and Fourier nonlinear parameters, thereby giving physical meaning to the Fourier parameters. Summing up, the intracycle coefficients represent coefficients describing the dynamic, local variations in the dissipative and elastic phenomena as a function of shear rate within an oscillation cycle.

MATERIALS AND METHODS

In this study, we investigated the rheological behavior of four finished formulation prototypes having unique textural properties. SAOS, LAOS, and other rheological data were generated for the four systems. The data obtained from rheology experiments were compared to textural data obtained by texture profile analysis. The validity of the instrumental techniques to accurately describe specific texture characteristics for each formula was challenged by sensorial analysis.

FORMULATIONS

Four distinct formulation systems were evaluated in this study, namely an alcohol-based sunscreen gel, a gel cream, an o/w SPF-15 cream, and an o/w emulsion with a higher wax phase.

Sunscreen Gel SPF-50. The product is created by gelling sunscreen filters, light esters (Ceraphyl™; Ashland, Inc., Covington, KY), and alcohol with lightly crosslinked poly(vinyl pyrrolidone) (FlexiThix™; Ashland, Inc.) (Table AI, Appendix 1).

Refreshing Gel Cream. This emulsifier-free o/w gel cream is created by combining two polymers, namely poly(acrylic acid/vinyl pyrrolidone) crosspolymer (UltraThix™ P-100; Ashland, Inc.) and cetyl hydroxyethylcellulose (PolySurf™ CS 67; Ashland, Inc.) with shea butter, light esters, and a few emollients (Table AII, Appendix 1).

Cushion Cream SPF-15. This bouncy o/w cream is achieved by combining lightly cross-linked poly(vinyl pyrrolidone) (FlexiThix™; Ashland, Inc.) with sodium polyacrylate (Covacryl MV 60; Sensient Cosmetic Technologies, Saint-Ouen-l'Aumône, France) and a mixture of nonionic and anionic emulsifiers, plus several ultraviolet filters and skin moisturizers (Table AIII, Appendix 1).

Buttery Cream. This o/w buttery texture is achieved by the combination of a lamellar gel technology based on glyceryl stearate (and) behenyl alcohol (and) palmitic acid (and) stearic acid (and) lecithin (and) lauryl alcohol (and) myristyl alcohol (and) cetyl alcohol (Prolipid™ 141; Ashland, Inc.), various long-chain esters (Ceraphyl™; Ashland, Inc.), and a relatively hydrophobic polymer, cetyl hydroxyethylcellulose (Natrosol™ Plus; Ashland, Inc.). A secondary polymer (Stabileze™ QM; Ashland, Inc.) is also added to the water phase of this cream for enhanced stabilization (Table AIV, Appendix 1).

RHEOLOGICAL CHARACTERIZATION

The rheological properties of the four prototypes were characterized using a strain-controlled ARES-G2 rheometer and a stress-controlled AR-G2 rheometer (TA Instruments, New Castle, DE). Rheological tests (n = 3) were carried out at 25° ± 0.1°C and 32° ± 0.1°C. Fresh samples were used for each test, and zeroing of the transducers was carried out before each trial to make certain that Lissajous overlays were repeatedly centered at the stress versus strain (shear rate) origin. Data analysis was completed using TRIOS software with the FT Analysis option, and Rheology Advantage (TA Instruments). To minimize structural changes or introduction of air bubbles during sample loading, an unvarying routine for sample loading was applied. The sample was scooped onto the bottom plate, after which the top plate was slowly lowered to the gap at a rate of 0.05 mm/s. After adjustment of the gap ($H = 1.00$ mm) and a 2-min equilibration to alleviate excess normal forces ($N_f < 10$ g), the sample edges were trimmed to minimize edge effects. Before data collection, a 3-min delay was applied to ensure replenishment of the compromised structure. Both smooth and rough plate surfaces were used for most rheological testing to evaluate how the contribution of edge effects, wall slip, shear banding, and/or plug-flow processes contribute to the meaning of the data. When rough plate surfaces were used, the sandpaper was changed after every trial. Details of the methodology for the employed rheological measurements are discussed in the sections below.

Dynamic strain sweep. Using the ARES-G2 and smooth plates, the oscillation amplitude was ramped from 0.1% to 600% strain at both 25° and 32°C to probe the effect of temperature on the *length of the LVR plateau*; the experiments were completed at 1 and 50 rad/s to see the effect of the applied frequency (and oscillation shear rate) on the results. The 2nd (I_2/I_1), 3rd (I_3/I_1), 4th (I_4/I_1), and 5th (I_5/I_1) harmonic intensities were followed as a function of oscillation strain. Higher order harmonics (e.g., I_2, I_3, I_4, I_5) typically appear with the onset of nonlinear changes in the sample structure. Even harmonics (e.g., I_2, I_4) are useful indicators for identifying the presence of asymmetrical wall slip, shear banding,

sample loss, and yield, as well as other nonperiodic flow instabilities—where dynamic oscillation of the material invokes an asymmetrical stress response to the direction of the applied strain oscillation. Odd harmonics (e.g., I_1, I_3, I_5), on the other hand, reflect symmetrical stress responses, such as homogeneous changes in microstructure, which are independent of the direction of oscillation.

Dynamic frequency sweep. Using the ARES-G2 and 25-mm parallel plates (smooth and rough surfaces), frequency sweeps were applied at 25° and 32°C to gauge the inherent *viscoelasticity* as a function of time, where time is inversely proportional to $1/f$. The angular frequency was swept from low to high (0.1–100 rad/s) within the LVR ($\gamma = 1\%$ strain) and, in other experiments, well outside the LVR ($\gamma = 50\%$).

Preshear and recovery. Experiments were performed using the ARES-G2 rheometer. The method involves preshearing the sample at a moderate shear rate, followed by a dynamic time sweep to monitor the rebuilding of structure as a function of time. The time dependence of structure rebuilding is related to *thixotropy*. Using both smooth and roughened surfaces, the following settings were applied: preshear = 20 s^{-1} for 180 s; recovery = dynamic time sweep (10 min, 1% strain, 1 rad/s) to monitor trends in G' as a function of time.

Steady torsional. Steady torsional experiments were performed with smooth and rough surfaces using the ARES-G2 rheometer. The shear rate was stepped to 20 s^{-1} and held steady for 300 s; trends in stress and viscosity were followed as a function of time. The test was performed to monitor *thixotropy*, which is time-dependent shear thinning.

Step stress growth. The step growth experiment was performed using the ARES-G2 rheometer. The test is transient, where an instantaneous shear strain rate is applied to gauge the *initial elasticity*. The shear rate was instantaneously stepped from 0 to 50 s^{-1} and held constant for 300 s using both smooth and rough plate surfaces.

Stress ramp. The steady stress ramps were performed using the AR-G2 rheometer. Stress ramps were applied with a stress-controlled rheometer to directly assess the *apparent yield stress* (τ_0) and *zero shear viscosity* (ZSV) of each material. All four cosmetic formulations exhibit apparent yield stress responses, meaning that their dispersed skeletal microstructures were strong enough to appear solid-like in a jar, and that they actually tend to creep or flow very slowly under the application of miniscule shear stresses (i.e., long deformation times). Consequently, the associated flow curves portray a ZSV plateau rather than an infinite viscosity in the limit of zero applied shear rate. Furthermore, only smooth surfaces were studied, so wall slip and plug flow values are comingled in the reported apparent yield stress values; hence, in the report "yield stress" is sporadically used, but the data are more accurately termed as "apparent yield stress events." The yield stress was measured at both 25° and 32°C to see the effect of temperature on the τ_0 and potential correlation with cushion and initial spreadability. The conditioning step included thermal equilibration followed by the application of a small stress (0.100 Pa) for 2 min to build up stress in the material. The shear stress was then ramped from 0.010 to 200 Pa. For each stress measurement, the maximum point collection time was limited to 1 min to curtail drying of the sample at the gap edge.

Brookfield viscometry. The *apparent viscosity* of the formulations was measured with a Brookfield RVT viscometer and the appropriate T-Bar spindle (Brookfield Engineering Laboratories, Inc., Middleboro, MA). The measurement was recorded after equilibrating at 5 rpm and 25°C for 1 min.

LAOS experiments. Using the ARES-G2, dynamic strain sweeps were applied using 25-mm stainless steel parallel plates ($R = 12.5$ mm) with both smooth and rough surfaces to ascertain the impact of wall slip on the oscillatory stress response. The rough surface was prepared by applying adhesive-backed, 400-grit sandpaper (ARC Abrasives, Inc., Troy, OH) to the top and bottom plates. To attain shear rates more applicable to spreading, the strain sweep was performed at the following settings: transient mode, 1–600% strain, 7 points/decade, 25 half cycles, 128 points/cycle, 2 delay cycles (2 s), $\omega = 50$ rad/s. Note that ordinarily 10–50 delay cycles are used to measure rheological properties of a sample at steady state; however, in this study, only two delay cycles were programmed to more realistically approximate the spectrum of microstructural breakdown as a function of successive iterations at the same shear rate, as well as increasing shear rates. Although some small inaccuracies subsequently propagate to FT analyses for samples exhibiting inherent thixotropy, the very small accuracy loss was less important than monitoring the complete microstructural breakdown of the probed sample. In separate experiments, the presence of wall slip, plug flow, and shear banding were crudely characterized by using an iPhone 5s camera (Apple Inc., Cupertino, CA) and a painted marker to assess the visual deformation of the vertical marker as a function of shear rate and angular displacement (see References 12 and 17 for a more rigorous analysis). Nonlinear properties were assessed with the TRIOS FT Rheology accessory software package (TA Instruments). The influence of electrolyte was examined by delivering 500 nmol/cm^2 sodium chloride (ACS reagent; Aldrich Chemicals, St. Louis, MO) from methanol (ACS reagent, Aldrich Chemicals) to the stainless steel surface of the top plate (transducer side). The treated plate was then predried at 32°C in the ARES-G2 oven before zeroing the geometry gap. Lissajous plots were subsequently generated using the aforementioned strain sweep methodology. Finally, a second set of lower oscillatory shear rate tests was performed to produce Lissajous plots for better visualizing microstructural changes in the apparent at-rest state. The low-frequency strain sweeps were executed with the following settings: transient mode, 1–600% strain, 7 points/decade, 25 half cycles, 128 points/cycle, 2 delay cycles (2 s), $\omega = 1$ rad/s.

TEXTURE PROFILE ANALYSIS

Texture profile analysis (TPA) was carried out using a TA.XTPlus Texture Analyzer distributed by Texture Technologies Corp. (Hamilton, MA) and manufactured by Stable Micro Systems (Godalming, Surrey, United Kingdom). It is equipped with a 5-kg load cell with 0.1 g force sensitivity. The Texture Analyzer is essentially a mechanical device with a probe attached to the load arm. Formulations were placed in a sample cell underneath the probe and were subjected to oscillating compression-tension deformation cycles by the probe. A cylindrically-shaped acrylic probe (TA-11; Texture Technologies Corp., Hamilton, MA) was used for the analyses. Typical settings were as follows: probe speed, 1.0 mm/s; deformation, 2.0 mm; deformation time, 1 s; and initial trigger force (point where the 1.0 mm deformation begins), 2 g. Data analysis was conducted with Exponent v6.14.0 software from Stable Micro Systems (Godalming, Surrey, United Kingdom).

SENSORIAL ANALYSIS

A five-membered expert panel completed the sensorial analyses. The formulations were evaluated for three distinct sensorial attributes: initial, middle, and finish rub-in. An

overall sensorial evaluation was captured for each of the formulations tested. The panel analyzed several sensorial parameters, including cushion, quick break, slip, tack, absorption, and finish on skin. Each parameter was evaluated on a scale from 1 to 10.

RESULTS AND DISCUSSION

Four formulations with distinct textural attributes were investigated by carrying out a battery of rheology tests, TPA, and sensorial analyses. Rheological analyses consisted of both traditional and novel, nonlinear (LAOS) approaches. Traditional methods included stress ramps, steady torsional, dynamic strain sweeps, dynamic frequency sweeps, and preshear and recovery experiments for generating materials characteristics such as apparent yield stress, ZSV, elastic modulus [$G'(\omega)$], loss modulus [$G''(\omega)$], complex viscosity [$\eta^*(\omega)$], and tan delta [tan $\delta(\omega)$]. Overall, these data revealed a number of important properties about the four texture formulations, related to their at-rest properties, which are reviewed in the Standard Rheology section below. During LAOS testing, each of the texture formulations uniquely responded to the deformation stresses required to realize the high-oscillation shear rates. The resulting Lissajous plots correlated well with initial sensorial parameters, especially quick break and cushion. Finally, this report is supplemented with a section on TPA, which is another instrumental approach that provides an alternative view of formulation textural properties, and a good determination of firmness, compressibility, resilience, and several other parameters.

To mitigate complications, parallel discs were chosen for all experiments as three of the tested systems contained emulsion particles that could interfere with smooth flow in a cone and plate truncation gap. For parallel discs, the calculated strain is proportional to R/H, where R is the plate radius and H is the sample gap. Hence, the equation implies that the applied shear rate varies with the volume of sample, and that the maximum applied shear rate only appears at the trimmed outer edge. This relationship is key because visualizing the edge of the sample conveys knowledge about how the sample relieves or stores the maximum applied oscillatory energy. Basically, this is where nonideal flow and deformation phenomena such as wall slip, plug flow, thixotropy, the coexistence of both soft solid and a liquid in yield stress materials, and shear banding may be visually observed—each of these processes affects the meaning of the measured stresses and, hence, the interpretation of the LAOS data and subsequent correlation with sensorial analyses.

BRIEF SUMMARY OF STANDARD RHEOLOGY DATA

The elegance of LAOS studies can only be realized in light of data captured from standard rheological methods. Standard rheological techniques were applied to provide a framework to better comprehend the meaning of the dynamic contours in each Lissajous plot. Where practical, samples were studied with both smooth and rough plate surfaces to assess factors such as wall slip. Results from stress growth and stress ramp yield stress (τ_0) experiments are possibly related to the low-strain internal loops of the Lissajous curves, and it is expected that each of these properties may have a subsequent relationship with the initial tactile properties, such as pick up, cushion, body, and initial spreadability. Steady torsional and preshear and recovery testing were undertaken to evaluate thixotropy, as thixotropic behavior could impact successive iterations at a single strain (or shear

rate), as well as the trajectory of loops at subsequent strains (or shear rates). Dynamic frequency sweeps were done to assess the time-dependent behavior of each formulation—where time dependence is related to the intrinsic relaxation behavior of the composite sample. Frequency sweeps in the LVR were compared to those commenced at 50 rad/s, which, in combination with larger strain amplitudes, results in large increases in the oscillatory shear rate. Unless specifically mentioned, the rheological outcomes relate to 25°C, smooth surface data.

The Sunscreen Gel SPF-50. It is an alcohol-based sunscreen gel that is thickened with lightly crosslinked poly(vinyl pyrrolidone) and packaged as a pump. Standard rheology shows that the Sunscreen Gel SPF-50 exhibits an apparent yield stress (14 ± 1 Pa) and shows slight thixotropy after yield, as evidenced by steady torsional and preshear and recovery experiments with both sandpaper and smooth surfaces. The smooth surface results differ slightly with the sandpaper data, indicating the presence of minor wall slip (below $\gamma = 2.5\ s^{-1}$), which is visible only at very low stresses ($<\tau_0$). The transient stress growth overshoot maximum was 239 and 206 Pa for the rough and smooth surfaces, respectively, suggesting a slight wall slip/shear banding process. Using a marker to monitor the deformation, it was difficult to visualize wall slip; however, it was clear that at postyield the sample begins to shear band, meaning that the sample volume flows in the gap, and that there is also a region near the center of the gap that flows at a higher shear rate than the bulk. Plotting the I_2/I_1 harmonic ratio in the dynamic strain sweep shows that I_2/I_1 decreases from 0.27 ($0.25\ s^{-1}$) to 0.01 ($5.0\ s^{-1}$). One possibility is that yielding of the microstructure is somewhat random, temporarily forming blobs of gel in a matrix of structured fluid, or that nonperiodic shear banding affects the low shear rate data. At 32°C isotherm, the I_2/I_1 harmonic ratio values ranged from 0.44 ($0.25\ s^{-1}$) to 0.02 ($5.0\ s^{-1}$); the uptick in I_2/I_1 at 32°C may be related to heterogeneous solvent evaporation (ethanol). At each isotherm, the I_2/I_1 ratio bottoms out at 0.008 before the end of the LVR. As indicated in Figure 3, the length of the LVR plateau at 32°C is not highly affected by dynamic shear rate. Post yield, I_3/I_1 increases monotonically for both 25° and 32°C isotherms. Further, once the gel yields, it readily flows at both low and high shear rates (which is mimicked *in vivo*). The ZSV and yield stress outcomes are not significantly affected by temperature. At 1% strain, the frequency sweep data conveys that $G' > G''$ over the entire tested frequency range, indicating the stability of the physical network; however, unlike the Refreshing Gel Cream, tan δ rises at higher frequency, demonstrating a shear rate dependence of the microstructural strength.

The Refreshing Gel Cream. It is an oil-in-water gel cream that is packaged as a pump. The standard rheology suggests the presence of minor wall slip (see below), along with the possibility of plug flow (i.e., the system moves as a discontinuous domain), which may exist before complete yielding ($\tau_0 = 66 \pm 3$ Pa). Observations with a marker did not reveal the presence of slip at the edge, but it is probable that the cohesive sample plug flows at lower shear rates, especially below the yield stress (as noted in dispensing product from its pump chassis). The transient stress growth overshoot maximum was 294 Pa for rough and 271 Pa for smooth discs, suggesting a slight wall slip or plug flow contribution. Plotting the I_2/I_1 harmonic ratio and the dynamic strain sweep shows that the ratio decreases from 0.14 ($0.25\ s^{-1}$) to 0.005 ($5\ s^{-1}$); the spike in $I_{2,4}/I_1$ suggests the presence of flow asymmetry at very low shear rates—which may be indicative of the cohesive nature of the Refreshing Gel Cream below yield. At each isotherm, near the end of the LVR and the

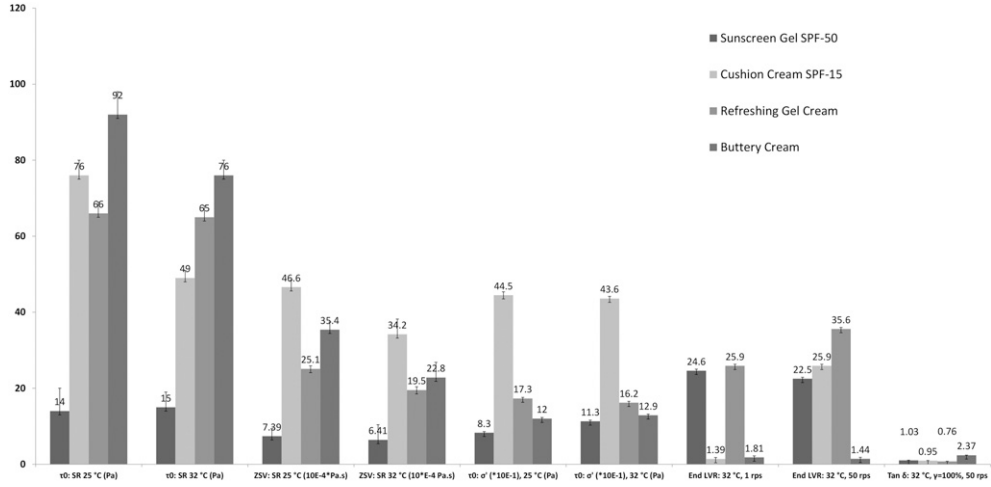

Figure 3. Summary of selected standard rheological results (smooth surface). SR = stress ramp result; End LVR (%) = approximated with intersecting lines method.

onset of the apparent yield stress (peak in elastic stress), I_3 and I_5 steadily rise. There is also evidence of very minor thixotropy, with a slight downward trend in stress as a function of time in steady torsional experiments (with and without sandpaper). Figure 3 also shows that the intrinsic cohesiveness of the Refreshing Gel Cream might influence the tan δ values and LVR plateau, where both values suggest the presence of a stable microstructure; hence, considering all minor effects, the rheological changes affecting sensorial appeal for the Refreshing Gel Cream are almost certainly related to direct changes in the dynamically shearing microstructure. Evidence of the microstructural stability in the LVR is visible in the frequency sweep data, which show that G':G'' > 10:1 and that G' and G'' are essentially parallel across the tested frequency range.

The Buttery Cream. It is provided in a jar, meaning that the user retrieves the product, more than likely, with the fingers. As the surface of fingers and skin are typically warmer than ambient conditions, the impact of temperature on the sensorial experience is critical. The apparent yield stress, as judged by stress sweep methodology, was $\tau_0 = 92 \pm 6$ Pa. Standard rheological methods for evaluating thixotropy (preshear and recovery, steady torsional) showed a decrease in viscosity as a function of steady shear rate, taking more than 5 min to recover from preshearing. By using a marker, it was shown that the sample plug flows at 25°C, meaning that the sample slips at both walls of the discs instead of uniformly deforming; hence, the total stress plateaus because the energy of the motor is no longer fully translated to the entirety of the sample. The transient stress growth overshoot maximum at 25°C was 1560 Pa (highest magnitude of all four prototypes) for rough and 1006 Pa for smooth discs (±10 Pa), corroborating the manifestation of plug flow. Steady torsional data from smooth and rough surfaces also showed that wall slip is present at low shear rates. Because low shear rates correspond to very initial spreadability, cushion evaluation, etc., slip layers are important factors in correlating rheology with sensory perception. At 25°C, the I_2/I_1 harmonic ratio also suggests some small asymmetric flow at oscillatory shear rates less than 4 s^{-1}. Below yield, the small asymmetric contributions from the even harmonics may be indicative of the formation of a smooth and consistent slip layer.

Temperature has a large impact on the firmness, flow, thixotropy, and subsequent sensorial properties of the Buttery Cream. At 32°C, τ_0 drops to 76 ± 4 Pa, which is a lower magnitude drop than expected, suggesting that the consistency and viscoelasticity of the slip layer dominates the apparent stress response of the rheometer at each isotherm. The tan δ value at 32°C, 50 rad/s, and 100% strain (strain sweep data), which is outside the LVR, but directionally pertinent to *in vivo* applications, is 2.37 ± 0.20, and expresses a fluid-like state (i.e., tan $\delta > 1$). Compared to other samples, at 32°C, the length of the LVR plateau is only slightly affected by frequency, indicating that temperature, rather than solely deformation time or dynamic shear rate, greatly dictates the physical state of the butter. At 25°C, 1% strain frequency sweep (i.e., LVR), no modulus crossover is seen for the Buttery Cream, where $G' > G''$ for the entire frequency range; tan $\delta < 1$ infers the stability of the Buttery Cream in the chassis, as well as the cohesiveness of the internal network within the LVR. An additional frequency sweep was performed on the Buttery Cream outside the LVR, at 50% strain and 32°C; although referring to dynamic moduli produced well outside the LVR is tenuous at best, the trends are being used to render a rough, directional comparison between microstructures. The frequency sweep with higher-magnitude strain was used to mimic reality, and clearly demonstrated that warming the formulation affects the rheology control of the waxy matrix—tan δ varies from 6.0 at 0.1 rad/s to 2.0 at 100 rad/s, indicating that the Buttery Cream is disposed to a much softer and flowing state on the surface of warm skin. Relative to 25°C, the I_2/I_1 (0.03) slightly increases at 32°C; this may be related to the onset of heterogeneous melting transitions in the waxy matrix.

The Cushion Cream SPF-15. It has a mousse-like texture and is packaged in a jar. The standard rheology data show that the apparent yield stress, as judged by standard stress sweeps, is $\tau_0 = 76 \pm 4$ Pa, and that the ZSV for the Cushion Cream SPF-15 is higher than the other textures, including the Buttery Cream, indicating that the Cushion Cream SPF-15 has more apparent viscoelasticity as the material builds stress and initially flows at near-zero shear rate. The τ_0 drops to 49 ± 2 Pa at 32°C, suggesting that thermal energy impacts the plate-sample interface during the lengthy application of very small stresses; the stress ramp to produce the yield stress data (Figure 3) is a slow test and shows that—given time—the Cushion Cream SPF-15 will slip at the smooth interface to offset the applied stress; this is also noted in the 32°C LVR plateau data, where, at lower frequency (1 rad/s), the plateau is similar to that of Buttery Cream. However, at higher frequency, the LVR plateau extends to 26%, indicating that the plate-formulation adhesion and the response and strength of the cohesive microstructure have a time dependency. In addition, the tan δ at higher strain and frequency is 0.95, indicating the texture of a gel-like state, rather than a fluid (in contrast to the Buttery Cream). The stress growth experiment shows an overshoot at 926 Pa for the sandpaper and 862 Pa for the smooth plates; again, at high shear rates, the Cushion Cream SPF-15 has a stronger structure, and the difference between smooth and rough surfaces is probably related to wall slip due to a more dominant inherent sample cohesiveness. As determined by preshear and recovery work, the level of thixotropy is insignificant, meaning that a very slight drop in the microstructural sturdiness fully recovers in less than 20 s. The LVR frequency sweep showed $G' > G''$ (G':G''~10:1) across the entire frequency range. In the 50% strain, 50 rad/s strain sweep at 32°C, which was also performed on the Buttery Cream, G' crosses G'' at 12 rad/s (~6.0 s^{-1}), indicating that the microstructural rigidity, and perhaps the interfacial response of the Cushion Cream SPF-15, are time dependent; at 32°C the internal structure is relatively less temperature dependent than the Buttery Cream and, hence, its rheological response may be more expected to

rival the rheological trends seen in the jar. Finally, at higher shear rates *in situ*, the Cushion Cream SPF-15 does peel from the parallel discs of the rheometer—evidently concurring that the formulation exhibits properties of cohesiveness. Note that, *in vivo*, interfacial phenomena and natural asperities aid in overcoming deleterious peeling or pilling of the formulation on the skin surface. At 25° and 32°C, the I_2/I_1 harmonic ratio suggests some asymmetric flow at oscillatory shear rates less than 1 s^{-1} (0.02 and 0.05, respectively); however, plug flow or slip was not seen with the application of a marker (25°C). At the end of the LVR, there were large and steady rises in I_3/I_1 and I_5/I_1 (0.08 and 0.02 at 100 s^{-1}), signifying nonlinear rheological changes. Finally, correlation of technology with the sensorial panel may be tricky for this sample as components of the initially thick-feeling Cushion Cream SPF-15 sorb fairly quickly into the skin, leaving behind a film with a nontacky, dry feel.

BROOKFIELD VISCOMETRY

As a reference point, Table I provides apparent viscosity and pH data for the four textural formulations. Generally, the pH values of skincare formulations are formulated as closely as possible to the skin surface pH in order to avoid incompatibility with skin flora. The viscosity data provide a general reference point for the formulations since Brookfield viscometry is employed almost universally in development and quality control laboratories. Removing the Buttery Cream result, the T-spindle Brookfield viscometry data correlated well ($R^2 = 0.988$ and 0.999, respectively) with the steady torsional and ZSV data for the Sunscreen Gel SPF-50, Cushion Cream SPF-15, and Refreshing Gel Cream. As the rheological data for the Buttery Cream were observed below the steady torsional and ZSV versus apparent viscosity correlation lines, this could indicate that the T-spindle results are less sensitive than rheometry to the generation of a significant interfacial slip layer for a sample structured with a waxy matrix.

SUMMARY OF NON-LINEAR RHEOLOGY DATA (LISSAJOUS REPRESENTATIONS)

Traditionally, dynamic oscillatory shear tests are conducted in the SAOS mode, and have been the preferred method to characterize the viscoelastic properties of soft solids. In recent years, however, much interest has focused on collecting data in the LAOS mode since many engineering, processing, and application operations often require impinging large deformation and higher shear rates on samples. As mentioned above, this certainly applies to preparations that are applied to the skin where the shear rates in spreading and

Table I
Brookfield Viscometry and pH Results (T Spindle, 25°C)

Formulation	T-spindle	Apparent viscosity (cP)	pH
Sunscreen Gel SPF-50	C	27,500 ± 2,500	NA
Cushion Cream SPF-15	D	95,000 ± 25,000	5.3 ± 0.2
Refreshing Gel Cream	B	42,500 ± 7,500	5.6 ± 0.2
Buttery Cream	D	185,000 ± 25,000	5.2 ± 0.2

rub-in can be enormous. Therefore, the four texture formulations were evaluated by means of LAOS. The reader should note that Lissajous plots from low frequency (i.e., lower oscillatory shear rate) experiments are also introduced in this section, as they illustrate many useful points when comparing the interaction of rough and smooth surfaces with the tested formulations. Figure 4 shows the viscous Lissajous plots from LAOS experiments for the four texture systems in the study. Most of the Lissajous plots in this article are viscous Lissajous plots of stress versus oscillatory shear rate. Each series of curves is plotted full scale so that the dynamics of the contours can be easily examined. Note that the ARES-G2 data are collected in transient mode, which means that the measured oscillatory shear rates are *instantaneous shear rates* and, hence, may not directly parallel trends in steady state shear rate data. Although traditional rheometry displays a collection of data points that may be taken as almost disjointed facts, the Lissajous plots convey a continuous flow of collective rheological changes.

The Sunscreen Gel SPF-50. As illustrated in Figure 4A, Sunscreen Gel SPF-50 has a smooth transition from an elastic microstructure (in the LVR) to a flowing, lightly structured fluid—as demonstrated by the evolution of symmetrical ellipses at the center to distorted ellipses with line-like "tails" at the highest strain rate. Figure 5A shows the impact of surface roughness on the measurement—where the rough surface displays higher total stress, thereby suggesting that wall slip, or, more likely, shear banding, confound the meaning of the smooth surfaces measurement at low shear rate. Hence, for the sandpaper, the transition of the Lissajous plots to thinner ellipses at higher strain rates suggests a plastic transition from a yield stress fluid. Although the yield transition in the prototypes

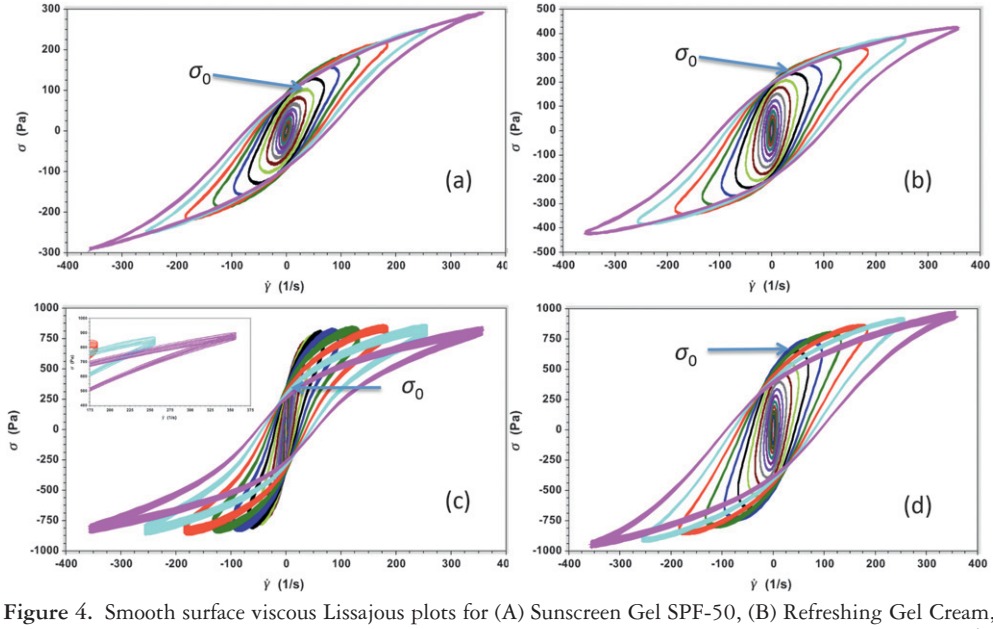

Figure 4. Smooth surface viscous Lissajous plots for (A) Sunscreen Gel SPF-50, (B) Refreshing Gel Cream, (C) Buttery Cream, and (D) Cushion Cream SPF-15 formulations. For the same applied strain, the inset in 4C shows stress changes with iterations of the same shear rate. Changes are related to the brittle and waxy microstructure, and the apparent thixotropy is accentuated at the highest oscillatory shear rates. σ_0 approximates the location of the apparent yield stress.

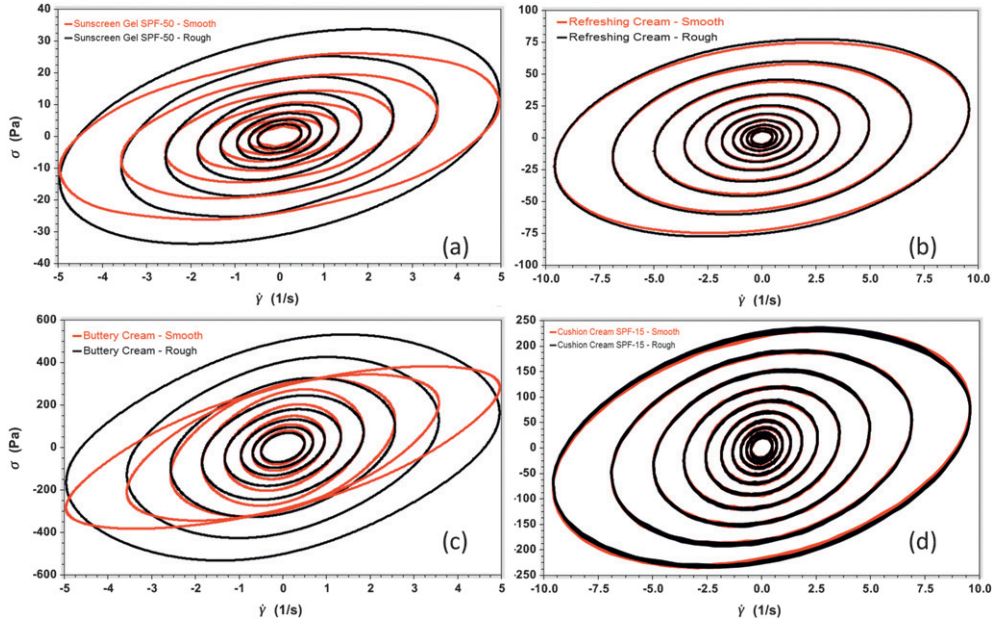

Figure 5. Smooth versus rough surface viscous Lissajous overlay ($\omega = 50$ rad/s) to emphasize the low oscillatory shear rate region for (A) Sunscreen Gel SPF-50, (B) Refreshing Gel Cream, (C) Buttery Cream, and (D) Cushion Cream SPF-15.

is less abrupt, and more of a gradual cascade in microstructural strength, experience with visualizing Lissajous trajectories enables a crude determination of yielding via LAOS (denoted as σ_0 or σ'_0 to differentiate from τ_0 from stress ramp data). These guesstimates may then be better confirmed by correlating critical loop shape changes with extracted G''/G' (σ_0) crossover data. For the 25°C/smooth data shown in Figure 4, the G''/G' crossover occurs at 116 Pa, which corresponds to loop 14, where $\sigma_{max} = 116$ Pa. A more reliable method may be to report the peak in σ' as a function of oscillatory strain (σ'_0), where $\sigma'_0 = 99$ Pa. It should be noted that σ_0 and σ'_0 calculated in this article are from high-frequency LAOS data and should not be confused with low shear σ_0 and σ'_0 data from low-frequency experiments, which may better correlate with shear ramp τ_0 data and subsequent assessment of the at-rest materials properties. Both yield stress results from the dynamic high-shear LAOS data (smooth surfaces) are substantially higher than that determined by standard stress sweeps (i.e., $\tau_0 = 14$ Pa), and are indicative of disparities in collective viscoelastic, slip, and shear banding responses while performing high-frequency LAOS experiments. Furthermore, yield stress materials do not obey the Cox–Merz rule; hence, oscillatory shear rate values obtained from dynamic experiments will never match those measured in steady state testing. The bending of the loops, and well-defined, superimposed lines between successive iterations at the same strain (compare to Buttery Cream; Figure 4C), suggest that the structure breaks quickly and reforms more slowly than the onset of the next strain setting; further, iterations at the same shear rate overlay, indicating very little to no thixotropy. The speed of the test to generate the Lissajous plot (<60 s) and the short delay between each strain increase (2 s) essentially conceal any significant structure rebuilding, which is apparently a longer-time process.

The impact of temperature is a factor to consider as the jar temperature normally varies from that of the skin surface. Figures 3 and 6A suggest that temperature (25° versus 32°C) only slightly affects the high-rate, shear-thinning behavior; however, although hidden in the scale of the overlay, this slight difference in total stress is accessible in G'_L/G'_M, Chebyshev elasticity index (e_3/e_1) and σ_{max} (Table II). Figure 7 maps the elastic component of the total stress (σ') as a function of shear rate. At the chosen isotherms using smooth surfaces, the effect of temperature on the apparent dynamic elasticity near the LVR is notable, but the difference is minimal at the highest shear rates, where mid-to-late spreadability is rated; hence, for smooth surfaces, the elastic contributions to the Sunscreen Gel SPF-50 sensory profile are expected to be similar at both 25° and 32°C isotherms. Note that shear banding and wall slip confound the physical meaning of the magnitude of σ and, therefore, σ', σ'', σ_0, and σ'_0. Nevertheless, wall slip is an integral part of the sensorial experience, and the *apparent* σ' is potentially more important to texture profiling than accurately gauging the true material property (i.e., slip or shear banding clouds the interpretation of the instrumental stress response).

The Refreshing Gel Cream. The Lissajous plots in Figures 4B, 5B, and 6B summarize the smooth, rough, and thermal data. The Lissajous trajectory of the Refreshing Gel Cream (Figure 4B) shows a smooth transition from a viscoelastic gel to a structured fluid, as judged by its nearly circular center loops and its thin Lissajous tail. Thermally speaking, the standard rheology (see Figure 3) of the Refreshing Gel Cream, including the apparent yield stress, was not affected by raising the temperature from 25° to 32°C; however, there was a decrease in the ZSV at the warmer temperature, indicating that the flow and associated molecular interactions at near-zero shear rate are slightly affected by heat. This is echoed in Figure 6B, which shows a very slight change (earlier stress plateauing) in the

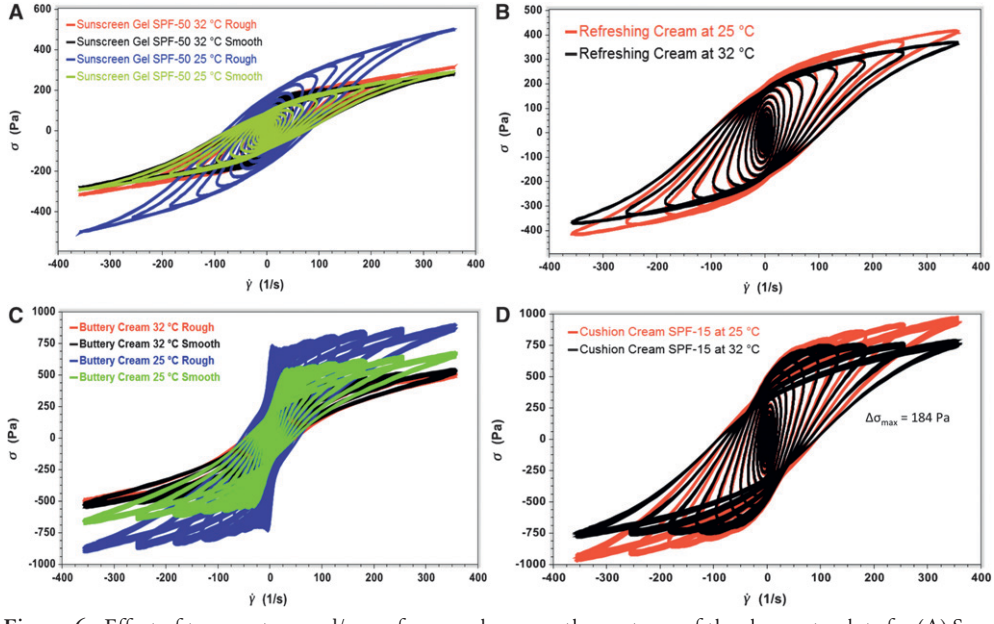

Figure 6. Effect of temperature and/or surface roughness on the contours of the shear rate plots for (A) Sunscreen Gel SPF-50, (B) Refreshing Gel Cream, (C) Buttery Cream, and (D) Cushion Cream SPF-15.

Table II
Summary of Nonlinear Rheology Data for 25°/32°C (Smooth Surface)

Formulation	G'_L/G'_M 25/32°C at 185 s^{-1} (±3.9%)	(e_3/e_1) 25/32°C at 185 s^{-1} (±0.01)	σ'_{max}, $\gamma = 600\%$ 25/32°C (±2 Pa)
Sunscreen Gel SPF-50™	4.80/2.45 (−43%)	+0.31/+0.23 (−26%)	177/126 (−29%)
Cushion Cream SPF-15	2.87/2.70 (−5.9%)	+0.24/+0.24 (0.0%)	400/336 (−16%)
Refreshing Gel Cream	3.52/2.57 (−27%)	+0.23/+0.23 (0.0%)	191/180 (−5.8%)
Buttery Cream	2.17/1.30 (−40%)	+0.26/+0.13 (−50%)	358/146 (−59%)

32°C Lissajous profile. Chebyshev and DFT analyses show that e_3/e_1 remains the same, but that there is a modest change in the nonlinear moduli ratio (G'_L/G'_M; Table II). The G'_L/G'_M ratio is very sensitive to slight changes in the tail shapes of the Lissajous curve; hence, the slightly lower stress plateauing in the 32°C stress curve (Figure 6B) is partially a function of changes in strain-induced stored energy as a function of temperature and shear. Similar to the Sunscreen Gel SPF-50, the Lissajous profile of the Refreshing Gel Cream (Figure 4B) describes a sigmoidal total stress versus shear rate profile, implying a transition from a soft solid to a structured fluid; however, relative to the Sunscreen Gel SPF-50, the magnitude of the maximum oscillatory stress at the highest shear is 130 Pa greater for the Refreshing Gel Cream; further, although the Sunscreen Gel SPF-50 is viscoelastic, the system trends toward a Newtonian fluid at ~300 s^{-1}, whereas (as evidenced by the larger area of the Lissajous tail in Figure 4B and the slightly larger area in Figure 7A) at higher shear rates, the Refreshing Gel Cream maintains a more appreciable degree of elasticity. Comparing the slopes of the inner ellipses of each system, which correlate with lower-shear texture properties, the microstructure of the Refreshing Gel Cream appears stiffer and more viscous with a longer LVR than the softer Sunscreen Gel SPF-50 (Figure 4A vs. 4B). The trend is inferred from the hurried deformation of circular trajectories of the Sunscreen Gel SPF-50, relative to the Refreshing Gel Cream technology, as observed at strain rates less than 4 s^{-1} (Figure 5, roughened surfaces data). Undoubtedly, there is not only a transition from circular to elliptical shape, but also a clockwise rotation of the loops (Figure 4A), implying softening of the Sunscreen Gel SPF-50 at relatively low deformation amplitudes—in a region where the Refreshing Gel Cream is nearer to its LVR. Finally, the apparent yield results from high shear rate LAOS (25°C, smooth surface plates) are 230/160 Pa (σ_0/σ'_0), which are higher than the Sunscreen Gel SPF-50 σ_0 data by

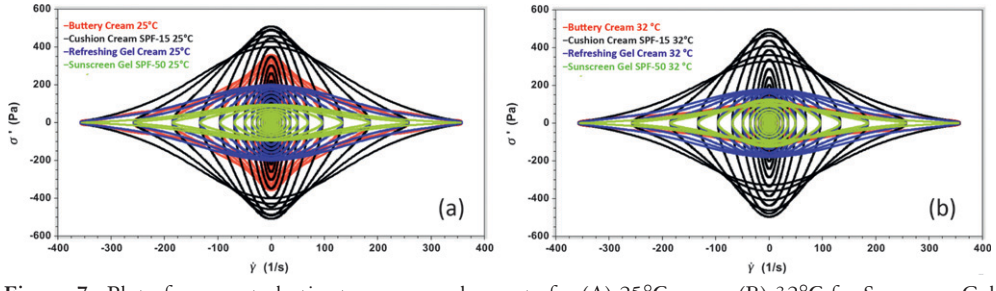

Figure 7. Plot of apparent elastic stress versus shear rate for (A) 25°C versus (B) 32°C for Sunscreen Gel SPF-50, Refreshing Gel Cream, Buttery Cream, and Cushion Cream SPF-15 (smooth plates). Note that wall slip and thixotropy are integral participants in the instrumental data as well as the sensorial ratings (12). Also, in 7B, note the diminished apparent elasisticity for the Buttery Cream.

150%. In contrast, in the stress sweeps, the Refreshing Gel Cream τ_0 result was 371% higher in magnitude than Sunscreen Gel SPF-50, and implicitly notes the time dependence of the microstructural response, as well as the impact of viscoelasticity on the corresponding apparent yield behavior.

The Buttery Cream. It is a system that behaves very differently in the jar than on the skin. Examining the Lissajous contour plot at 25°C (Figure 4C) and using smooth or rough plate surfaces, the Buttery Cream sample shows the highest stress of the four textures up to 150 s^{-1}, after which the structure begins to soften and, subsequently, the total stress plateaus. Comparing the higher shear rate data of the Buttery Cream to the Cushion Cream SPF-15, the total stress maxima are similar, but the Cushion Cream SPF-15 shows much more apparent elasticity, as noted by its wider contours at moderate-to-high oscillation shear strain rates (50–350 s^{-1}). There appears to be some time needed for measurement equilibration of the Buttery Cream, as per the striations and gradual stress decay for each iteration at a particular strain (see inset of Figure 4C), which was paralleled by standard rheological methods for evaluating thixotropy (i.e., preshear and recovery, steady torsional). By using a marker to visually follow the deformation within the sample gap, it was shown that at 25°C the sample plug flows, meaning that the sample slips at both walls of the discs instead of laminarly deforming; hence, the total stress plateaus because the energy of the motor is no longer fully translated to the entirety of the sample. Further, as noted from comparisons of smooth and rough surfaces data, wall slip and plug flow affect the tilt and maxima of the smooth-surface Lissajous loops. It appears that generated slip layers lead to lubricity and increased plug flow. For the Buttery Cream, the generation of slip layers is an important factor in correlating rheology with sensory perception.

Temperature has a large impact on the firmness and spreadability of the Buttery Cream (Figure 6C). In fact, the Buttery Cream appears to melt onto the skin almost immediately, showing that for structured waxes it is key to study rheology at the temperature pertinent to the application (e.g., skin = 32°–35°C) (18). At 32°C, the stress at maximum shear strain rate drops by 302 Pa, meaning that the amount of apparent viscoelasticity decreases significantly on transition from ambient to the skin surface temperature; the same directionality is seen in the trends in σ' (elastic stress) as a function of shear rate. Figures 7A and B show that at 32°C, the level of the apparent (i.e., slip affected) elastic stress for the Buttery Cream drops below that of the Sunscreen Gel SPF-50, meaning that the elasticity of the Buttery Cream microstructure, even at low shear rates, is significantly softer than it is at 25°C.

The G''/G' crossover and σ'_0 yield stress results (25°C, smooth) from high-shear LAOS (394/293 Pa, respectively) suggest that the yield magnitudes from LAOS are three to four times higher than the standard stress sweep result (τ_0 = 92 Pa) and that at low strains ($\gamma < 3.7\%$) and short times, the waxy, crystalline microstructure is quite strong. Further, near the yield, higher oscillatory shear rates and the inability for the microstructure to relax may suppress inherent wall slip effects—thereby leading to a more accurate probing of the at-rest waxy microstructure.

The Cushion Cream SPF-15. The Cushion Cream SPF-15 and Buttery Cream have similar stress maxima in their final Lissajous loops (25°C, Figure 4C, and D, respectively); however, looking at the low shear rate data from smooth and rough surfaces (Figure 5C and D) shows that the Buttery Cream at 25°C has more initial elasticity than the Cushion Cream SPF-15. Interestingly, evaluating the σ' and σ'' data versus strain for both systems

clarifies what is happening; at higher strains the Cushion Cream SPF-15 has larger elasticity, viscosity, and total stress; but, when the Buttery Cream is in the LVR, its structure is quite strong. Like the Lissajous initial stress data (i.e., first few loops), the apparent yield stress (stress sweep data) of the Buttery Cream is also higher (τ_0: 92 ± 6 vs. 76 ± 4 Pa for Cushion Cream SPF-15), suggesting that the total stress at maximum strain in the Lissajous is not necessarily indicative of the energy needed to start the cascade of the microstructure; however, after sufficient strain is imparted to the Buttery Cream, even at ambient temperature, Figure 7A shows that the elastic stress for Cushion Cream SPF-15 overtakes that of the Buttery Cream at <50 s^{-1} and that the maximum elastic stress for the Cushion Cream SPF-15 (509 vs. 358 Pa) at the highest shear rate is greater than that of the Buttery Cream. At 32°C, as shown in Figure 7B, the level of elastic stress for the Buttery Cream drops below that of the softest texture in the study (i.e., Sunscreen Gel SPF-50), whereas the Cushion Cream SPF-15 maintains the strongest microstructure in the hierarchical comparison between the four textures. The LAOS crossover and σ'_0 yield stress data (25°C, smooth) show that σ_0/σ'_0 = 457/338 Pa, respectively; further, the G''/G' crossover occurs at γ = 138% (vs. 9.9% for the Buttery Cream), suggesting that at higher frequency the polymer-driven fine structure of the Cushion Cream SPF-15 is much more strain resistant than that of the Buttery Cream.

Figure 8 summarizes the Lissajous contours by examining basic trends in nonlinear parameters. Figure 8A shows G'_L as a function of shear rate. Trends in G'_L enable a means to monitor nonlinear intracycle elasticity, and are indicative of strain (shear rate)–dependent changes in the Lissajous loop shape. From the plot it is evident that the crystalline matrix of the Buttery Cream loses its ability to store energy at higher strains more quickly than the Cushion Cream SPF-15; whereas the Sunscreen Gel SPF-50 and Refreshing Gel Cream change similarly (same profile as Cushion Cream SPF-15, different total stress magnitudes). Table II provides a ratio of G'_L/G'_M, which facilitates an understanding of how the nonlinear elasticity is changing as a function of oscillating strain, or shear rate. In the LVR, G'_L/G'_M = 1; hence, at an oscillatory shear rate of 185 s^{-1}, each of these samples approaches more nonlinear behavior owing to changes in local elasticity and/or loss in structure. As noted by G'_L/G'_M trends at 25° versus 32°C, the Cushion Cream SPF-15 maintains a similar Lissajous shape. In contrast, the Sunscreen Gel SPF-50 and Buttery

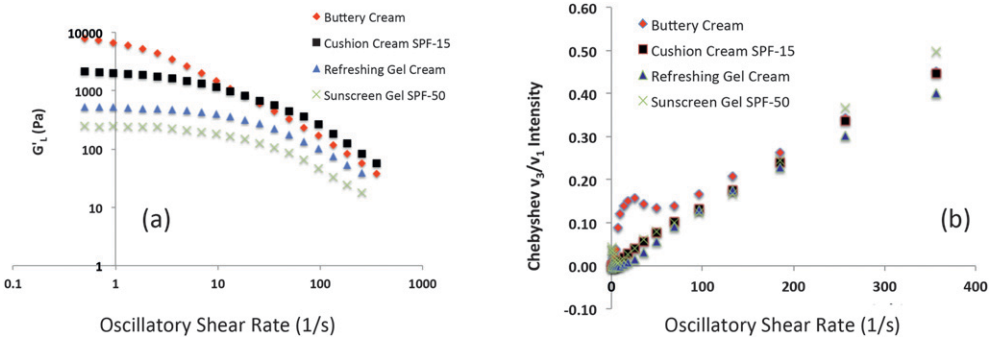

Figure 8. Effect of increasing shear rate on the (A) large strain modulus and (B) Chebyshev v_3/v_1 intensity ratios at 32°C for Sunscreen Gel SPF-50, Refreshing Gel Cream, Buttery Cream, and Cushion Cream SPF-15. For the Chebyshev plot, a positive sign suggests intracycle shear thickening, whereas a negative sign indicates intracycle shear thinning processes.

Cream are more highly affected by thermal energy—changing 43% and 40%, respectively. The e_3/e_1 and σ'_{max} follow the same proclivity.

Figure 8B shows trends in the third harmonic viscous Chebyshev coefficient intensity, v_3/v_1, as a function of shear rate. Positive v_3/v_1 values relate to intracycle shear thickening; $v_3/v_1 = 0$ implies linear viscous behavior, and $v_3/v_1 < 0$ relates to intracycle shear thinning. All four of the textures show intracycle shear thickening characteristics at low shear rates, possibly because the frequency is high and the strains are low, which may result in vibrating the structured fluid rather than shredding it. Eventually, an oscillation strain or shear rate amplitude (i.e., $\lambda_0 \cdot \omega$) is breached where the structure no longer has the means to support the deformation, and, therefore, flow begins. All four textures exhibit viscoplastic behavior, meaning that each system yields to a progressively cascading microstructure that leads to increased flow.

The Lissajous curves in Figure 9A–D represent the stress response to high deformation, but at lower angular frequency, and, hence, lower oscillatory shear rates than the experimental settings used to generate Figure 4. The inner loops in the viscous Sunscreen Gel SPF-50 Lissajous curve are upright and nearly circular (Figure 9A). The circular trajectory typically indicates an apparent elastic response; additionally, at shear rates less than 1 s^{-1}, the loops appear to rotate clockwise into deformed elliptical trajectories, indicating that the stress response is more in phase with flow. These low shear rate effects are partly due to very minor wall slip. In the no-slip region, at the maximum shear rate (~4 s^{-1}), the loop tips resemble those of near-Newtonian flow with some residual elasticity, and suggest that the integrity of the Sunscreen Gel-SPF-50 microstructure is very sensitive to large strain amplitudes. The apparent σ'_0 from low-frequency LAOS is 29 Pa, suggesting that low-frequency transient experiments more closely approximate the viscoelastic response

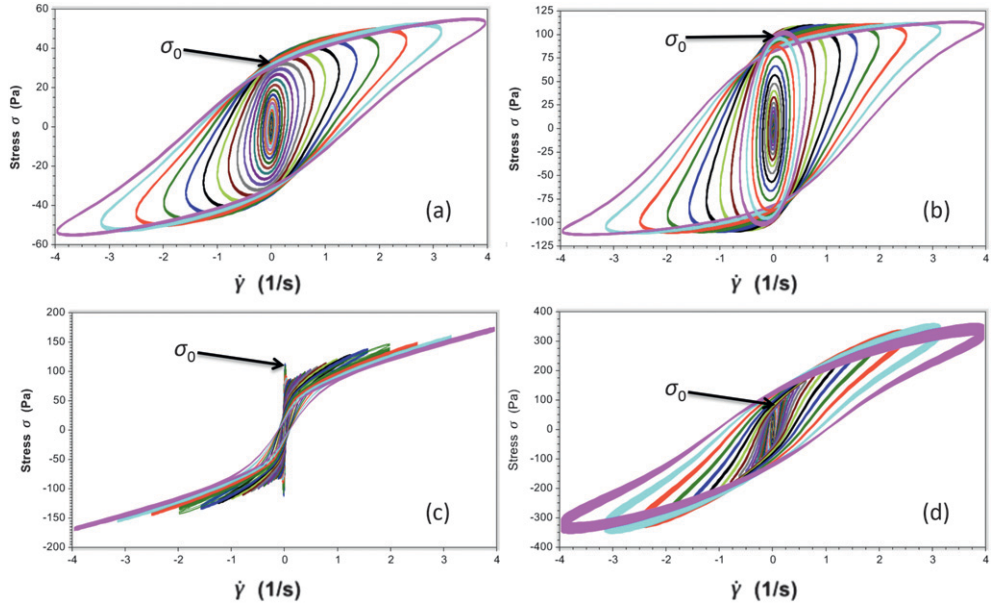

Figure 9. Lissajous plots for (A) Sunscreen Gel SPF-50, (B) Refreshing Gel Cream, (C) Buttery Cream, and (D) Cushion Cream SPF-15. The data were performed at $\omega = 1$ rad/s to more closely approximate changes in steady-state viscoelasticity. σ_0 approximates the apparent location of the apparent yield stress.

of the stress ramp data. Further, the rough and smooth data at 25°C and observations from marker data express that the inclination for shear banding is higher at ambient than at skin temperature—hence, the intensity of shear banding for Sunscreen Gel SPF-50 may be tied to temperature-sensitive gradients in microstructural strength. In contrast, the Refreshing Gel Cream (Figure 9B) responds with twice the maximum stress and with much more elasticity. At shear rates of $>1\ s^{-1}$, the physical network of the Refreshing Gel Cream bends but does not break. Figures 5B and 9B further imply that wall slip is indeed very minimal for the Refreshing Cream. The Lissajous profile shown in Figure 9B indicates the high elasticity, and the apparent σ'_0 from the low shear rate LAOS data (peak in elastic stress) is 93 Pa, rivaling that of the Cushion Cream ($\sigma'_0 = 102$ Pa). The prevailing line-like loop shapes in the Buttery Cream (Figure 9C) system are indicative of plug flow properties—where the slip layers flow and protect the waxy microstructure of the Buttery Cream from the full brunt of the applied strains. The vertical inner loops eventually portray yield ($\sigma'_0 = 63$ Pa), but the accuracy of the response is no doubt masked by interfacial slip. The Lissajous plot for the Cushion Cream SPF-15 in Figure 9D resembles that of a flowing fluid—clearly this illustrates the effects of low shear rates inducing slip and plug flow processes, where slip provided by the acrylic beads and cohesiveness from the polymeric-driven microstructure overwhelm the weaker plate-sample adhesion forces. One trend to note is the difference (Δ) between the high and low LAOS shear rate (σ'_0) yield data: Sunscreen Gel SPF-50 ($\Delta = 7$ Pa), Refreshing Cream ($\Delta = 7$ Pa), Cushion Cream SPF-15 ($\Delta = 24$ Pa), and Buttery Cream Cream ($\Delta = 23$ Pa). These data indicate that the response to imposed transient strain for the Cushion Cream SPF-15 and Buttery Cream are time dependent. Further, based on comparisons between the Lissajous plots in Figures 4 and 9, the responses are at least partially masked by interfacial slip and plug flow effects that no doubt partially translate to initial sensorial properties.

Electrolyte levels and pH impact the rheology of anionic thickeners, such as crosslinked poly(acrylic acid). The pH for optimum thickening is 6–7, and there is a precipitous decrease in bulk viscosity as the pH drops below 5.5. As the pH of the acid mantle of the stratum corneum typically ranges from pH 4–5, local interactions between the mantle and carboxylates may induce slight shifts in the interfacial rheology (19). Further, and perhaps more importantly, electrolyte levels vary from person to person and from season to season (20). Salt melting, which is caused by water-soluble cations interfering with the electrostatic thickening mechanism, profoundly impacts the rheology of anionic thickeners. As with pH, the effect on viscosity is localized at the interface, but may become more pronounced as an emulsion is broken down while shearing the product into the skin.

Ewoldt and McKinley developed a convention for using Lissajous plots to quantify the transition of a structured material to its flow state (21). Using the loop area in an elastic Lissajous plot, where the area relates to energy dissipation, it is possible to follow the gradual cascade of the microstructure and to relate the data to variations in measured stress—which is what the "transducer" of a panelist senses when rubbing a cosmetic formulation into the skin. In brief, the energy dissipated in a single oscillation cycle is compared to the maximum energy that can be dissipated in a perfect plastic response (ϕ)—where the maximum dissipated energy is visually described by the smallest rectangle (in a σ_{max} vs. γ_{max} plot) that each Lissajous loop can fit within. The scalar quantity, ϕ, is essentially a 2-D representation of microstructural changes as a function of shear. Like stress, ϕ is sensitive to wall slip and changes at the product–transducer interface, where salt melting occurs. A magnitude of $\phi = 0$ represents an elastic response, and $\phi = 0.785$

indicates Newtonian flow. A perfect plastic response, which is rare in a cosmetic formulation, produces $\phi = 1$.

Figure 10 compares data with no electrolyte to data at 32°C with 500 nmol/cm^2 of sodium chloride applied to the surface of the parallel plate (transducer side). It is apparent that σ versus ϕ data from the Lissajous contours, which has been plucked from a single Lissajous plot, distinguish the impact of salt on the stresses sensed by the instrument transducer. Other than the Sunscreen Gel SPF-50, all formulations have at least one chemical component that may be influenced by the presence of electrolyte. Without electrolyte, the Refreshing Cream, which contains an anionic thickener, shows a slow transition from a viscoelastic gel to a Newtonian fluid; however, the stresses appear much higher than the Sunscreen Gel SPF-50. In the presence of salt, the maximum stress drops from 463 to 279 Pa, putting the stresses of the Refreshing Cream nearer to that of the Sunscreen Gel SPF-50 (242 Pa). The Buttery Cream also contains an anionic thickener in its water phase; although the rheology of the water phase of an emulsion may be less affected by salt levels than a cross-linked polyacrylic acid thickened hair gel, it is evident that the stresses induced at higher shear rates are lower in the presence of the electrolyte. This could be related to increased surface area and the intended breakdown of the emulsion at higher shear rates. The σ versus ϕ gradient for the Cushion Cream SPF-15 formulation is different than the others and suggests a transition to flow, but with a higher stress response. Salt impacts the profile only at high ϕ, which may be related to slight changes in the size of the acrylate beads—thereby introducing the possibility of forming a lower viscosity slip layer.

At low strains, the even harmonic intensity salt data (I_2/I_1) was also followed to monitor asymmetrical wall-slip trends. For the salt data at 1% strain, the following values were obtained: Refreshing Cream (0.082); Sunscreen Gel SPF-50 (0.070); Cushion Cream SPF-15 (0.043); and Buttery Cream (0.022). Typically, the higher the magnitude of I_2/I_1, the greater the asymmetric flow; hence, interfacial slip, which may be a product of

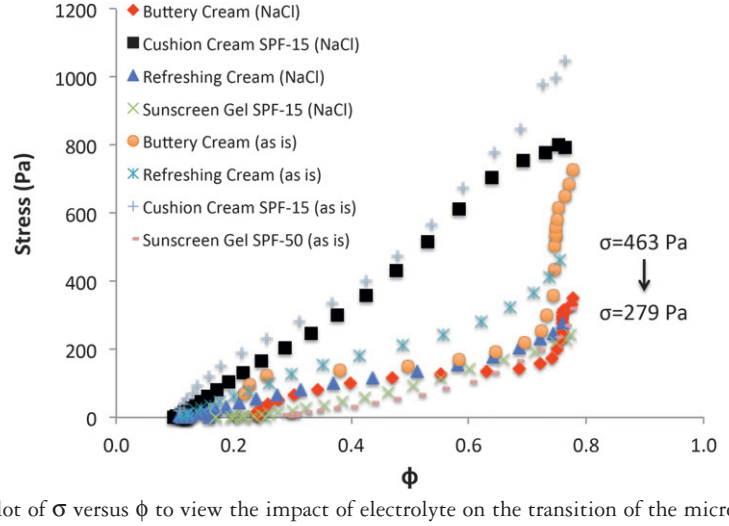

Figure 10. Plot of σ versus ϕ to view the impact of electrolyte on the transition of the microstructure to a nearly Newtonian fluid. Comparisons are made for systems tested at 32°C with no salt for Sunscreen Gel SPF-50, Refreshing Gel Cream, Buttery Cream, and Cushion Cream SPF-15.

electrolyte dynamically mixing from the steel–sample interface into the bulk, arguably adds asymmetrical structure and viscosity changes that may be conceivably comingled into the sensorial perception of slip. Interestingly, the Buttery Cream, which has the highest slip, has the lowest I_2/I_1—this points to more symmetry in the slip mechanism, and perhaps greater homogeneity of the sample within the sample gap.

TPA

TPA was carried out using a texture analyzer equipped with an acrylic, cylindrically-shaped probe. It is a very practical technique for characterizing the textures of cosmetic products. Creams, lotions, and gels available in the skin-care market can vary considerably in their textural properties. For example, a typical antiaging cream would be distinctly different from a body milk formulation. The antiaging cream normally would have much more consistency or structure as well as a distinct rub-out profile, cohesiveness, etc. The body milk, on the other hand, would spread very easily, even without additional external forces, such as spreading by fingers. These types of characteristics are captured in TPA experiments.

In a typical test, two compressive deformations are carried out during the course of TPA, resulting in two positive peaks (each peak corresponds to a deformation) in a force versus time profile (see Figure 11); (22). From the plot, we can calculate several parameters that

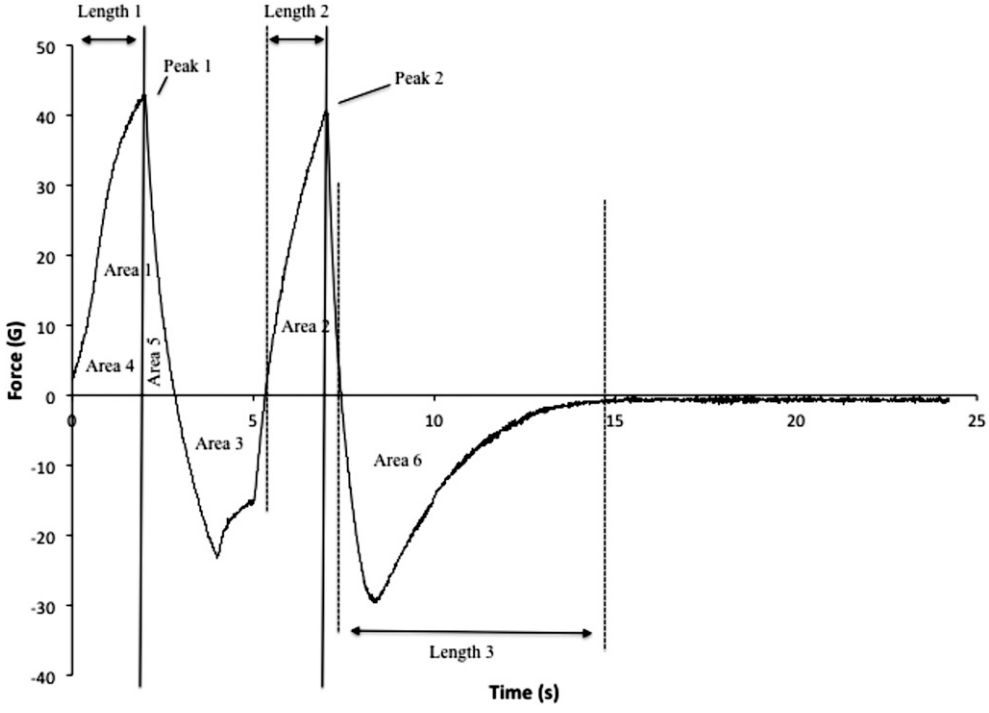

Figure 11. Example of a typical texture profile analysis curve denoting specific length, peak height, and area measurements used to calculate textural attributes.

can be related to textural properties of the formula. Areas 1 and 2 are the calculated areas under the first and second peaks, corresponding to the first and second deformations. These values are used to calculate the TPA cohesiveness (Area 2/Area 1) and compressibility [1 − (Area 2/Area 1)] of the emulsion. Peak 1 is the maximum value of the first peak and corresponds to the firmness or penetration force required to deform the sample. The first peak can further be analyzed by taking the ratio of Area 5 to 4, which provides a measure of resilience. During withdrawal of the probe, the force of attraction between the particles of a substance and the probe (adhesion) may be gleaned from Area 3 or 6 (negative peaks). Integrity of shape corresponds to the springiness of the sample and may be calculated by taking the ratio of Length 2 to 1. The elastic resistance to deformation for a semisolid corresponds to Peak 1 (Area 2/Area 1). Finally, stringiness corresponds to Length 3, which begins in the negative force region of Area 6 and ends when the force becomes asymptotic to zero force.

In this work, we characterized the four prototype formulas according to the various TPA results, which are shown in Table III. Upon inspection of the data, it is immediately apparent that firmness is the highest for the Buttery Cream followed by the Cushion Cream SPF-15, Refreshing Gel Cream, and Sunscreen Gel SPF-50. For comparison, the maximum stress values in Figure 4 from the LAOS experiments match very well with the firmness data for all of the formulas. The compressibility is a little more difficult to discern upon initial inspection. The Buttery Cream is the most difficult to initially penetrate, which may be attributed to the large quantity of esters and the rigid lamellar gel technology in the formula; however, the Cushion Cream SPF-15 is the most difficult to condense in successive compressions, essentially illustrating the objective design of this product as a "bouncy cream." Not surprisingly, resilience follows the same trend as compressibility, demonstrating that the Buttery Cream is thixotropic and that the Cushion Cream SPF-15 quickly adapts to changes caused by the initial force deformation. The TPA resilience data again resonate with the results of the thixotropy data from the steady torsional, preshear and recovery, and LAOS work; as opposed to the other three textures, apparently there is rapid structure breakdown, and/or perhaps the generation of an interfacial slip layer, for the Buttery Cream after the initial probe penetration. The Refreshing Gel Cream and Sunscreen Gel SPF-50 both exhibit higher compressibility and resilience than the Buttery Cream, which also suggests minimal thixotropy and rapid microstructure recovery.

Cohesiveness refers to the tendency of the molecules within the composite formulation to stick together and is given by Area 2/Area 1 in the TPA curve. Normally, formulas with significant consistency tend to be more cohesive. For example, a product that spreads or flows easily would tend to be less cohesive. Similar to the comparison we provided above—skin-care cream versus body milk—a skin-care cream would be more cohesive than a body milk. For the tested formulas, the Buttery Cream provides the highest cohesiveness followed by the Cushion Cream SPF-15, Refreshing Gel Cream, and Sunscreen Gel SPF-50. Interestingly, these data follow the same trend given by τ_0, which is not surprising as the yield stress and cohesive forces describe similar physical behavior related to the breakdown or flow of a material. The cohesiveness data inversely trend ($R^2 = 0.914$, semilog plot) with G'_L/G'_M at 185 s^{-1} (see Table II). As stated previously, G'_L/G'_M provides an indication of nonlinear Lissajous shape and is a measure of the ratio of the elasticity at large strains (G'_L) to the residual elasticity (G'_M) at 0% oscillatory strain. The resulting correlation suggests that lower TPA cohesiveness, which is derived from area of work

Table III
Selected Textural Attributes of the Tested Formulations (25°C)

Texture	Firmness	Compressibility	Resilience	Cohesiveness	Integrity of shape	Elastic resistance to deformation
Sunscreen Gel SPF-50	14.25 ± 0.78	0.79 ± 0.04	0.12 ± 0.01	23.57 ± 1.58	0.87 ± 0.02	11.27 ± 1.13
Cushion Cream SPF-15	105.25 ± 6.01	0.84 ± 0.01	0.18 ± 0.01	122.98 ± 12.62	0.85 ± 0.01	88.72± 3.98
Refreshing Gel Cream	39.75 ± 2.47	0.76 ± 0.00	0.15 ± 0.02	73.74 ± 7.45	0.79 ± 0.01	30.14 ± 1.95
Buttery Cream	127.85 ± 14.92	0.70 ± 0.00	0.08 ± 0.01	214.24 ± 18.44	0.90 ± 0.01	89.58 ± 10.26

measurements, relates to increasing nonlinearity; essentially, the Buttery Cream and Cushion Cream SPF-15 are more cohesive than the Refreshing Gel Cream and Sunscreen Gel SPF-50 technology, and the outcome may be interconnected with greater retained elasticity (at 25°C, 185 s^{-1}). Moreover, there is also a linear correlation ($R^2 = 0.967$) between σ'-LVR, which is the elastic stress isolated from the LVR, and TPA cohesiveness. The result implies that work energy derived from low frequency probe oscillations in TPA may best relate to linear deformation outcomes in LAOS. Another trend to note is that there is a logarithmic correlation ($R^2 = 0.997$) between Brookfield viscosity and cohesiveness—hence, both TPA and Brookfield viscosity measurements with a T-spindle may have negligible (or similar) sensitivity to wall slip.

The integrity of shape data—also reported in Table III—do not conform to basic rheological parameters but depend on the complex interactions of the product with itself and with the acrylic texture analyzer probe. The Buttery Cream has the highest values in this category followed by the Sunscreen Gel SPF-50, Cushion Cream SPF-15, and Refreshing Gel Cream. The elastic resistance to deformation seems to follow a trend related to the consistency of the sample that reflects the same trends observed for firmness and cohesiveness. This could be related to the original LAOS plots shown in Figure 4 by examining the maximum stress encountered at prescribed strains; however, this term is probably complex and depends on a number of physical factors of the formula.

In addition, comparing the instantaneous elasticity results from stress growth experiments obtained with the rough and smooth surfaces (Summary of Standard Rheology Data section) with the cohesiveness data from the TPA experiments, we find that the absolute differences follow the same trend as the cohesiveness data obtained from the TPA. For example, in the stress growth experiment, the following mathematical differences between rough and smooth surfaces are obtained: Sunscreen Gel SPF-50 (33 Pa), Refreshing Gel Cream (33 Pa), Cushion Cream SPF-15 (64 Pa), and Buttery Cream (554 Pa). As already stated, mathematical differences in the stress growth data more than likely indicate wall slip and reflect trends in interfacial properties as well as cohesiveness.

One should bear in mind that while similarities in trends may be observed between standard rheology tests and TPA, fundamentally, the mechanical deformation is distinct. In TPA, we investigated the texture of the formula during pickup from the packaging, since this technique is conducted in the z-direction, and with relatively low probe velocity, without consideration of shear forces. Nonlinear, high shear rate rheological techniques, on the other hand, provide better insight into the rub-out behavior of product, and are more accurately captured by LAOS techniques. Furthermore, the reported TPA experiments were conducted at 25°C; hence, using the generated TPA data to emulate the performance of the Buttery Cream on the skin (32°–35°C) is not entirely feasible.

SENSORIAL ANALYSIS

A five-membered expert panel carried out the sensorial analysis. Principally, they judged the initial, middle, and final rub-in profiles for each product and provided rankings for quick break, tack, cushion, slip, dry feel, quick absorption, and light feel. In addition, the expert panel provided a sensorial description of each formulation, which is also described in this section. Figure 12 depicts the sensorial evaluations for the four formulations. Ratings are from 1 to 10, where a value of 1 disagrees with the named characteristic while 10

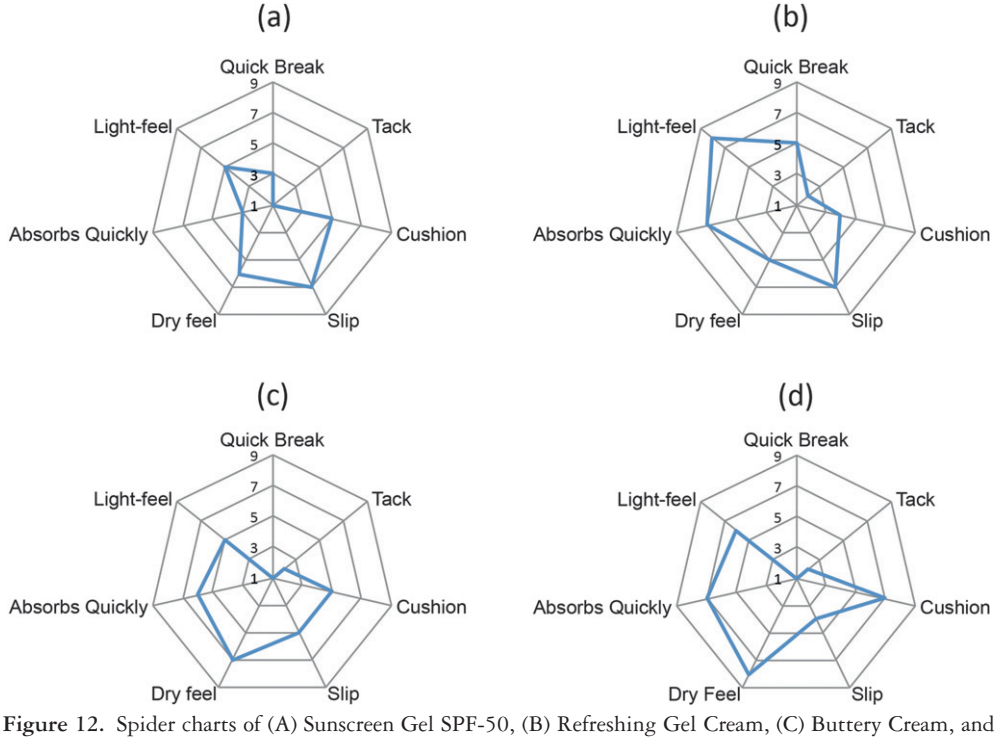

Figure 12. Spider charts of (A) Sunscreen Gel SPF-50, (B) Refreshing Gel Cream, (C) Buttery Cream, and (D) Cushion Cream SPF-15 representing the sensorial performance results that were tallied by a trained expert panel (n = 5). Each sensorial characteristic was ranked from 1 to 10, where a score of 10 is in complete agreement with the named parameter, e.g., a score of 1 for slip means very little perceived slip, whereas a score of 10 is the maximum perceived slip.

completely agrees. For example, for quick break, a value of 10 is assessed if the formulation breaks quickly during shear and is easily perceived, whereas 1 means it is difficult to sense a change in consistency. From the sensorial ratings data shown in Figure 12, slip, quick break, and cushion are the early-to-middle sensorial characteristics that are most suited for correlation with rheology and the parameters studied by TPA. Light feel appears to be a complex sensorial facet and is discussed later in the text (see page 32).

During the tactile evaluation, product was applied to the dorsal portion of the panelist's hand just above the upper thumb joint. While pressing down slightly with the index finger of the hand, a circular rubbing motion was made to evaluate each product. The Sunscreen Gel SPF-50 was characterized by panelists as having a soft, oil-like consistency, which uniformly glides on the finger. During initial rub-in, this product adapts a thickened, light-oily feel. The middle rub-in profile can be characterized as nonabsorbing, slippery, and nontacky. During rub-in, the Sunscreen Gel SPF-50 breaks down from a semisolid to a liquid, which is associated with a loss in viscosity; however, it is a gradual process. It does not have quick break characteristics, meaning there is no rapid change in feel. In addition, there is no tack associated with the formulation. Overall, the Sunscreen Gel SPF-50 does not absorb quickly (i.e., long play time) and tends to form a lasting thin film on the surface of the skin.

The initial tactile perception of the Refreshing Gel Cream is a "cool to touch" sensation. Pressing down with the index finger, it was noted that the product is adaptable and easy to manipulate. There is a slight cushion that is similar to that of Sunscreen Gel SPF-50. During rub-in, there is a perceptible quick break. It should be noted that quick break processes are usually observed due to a dramatic change in feel that is associated with a discernible variation in the structure of the product, resulting in a cooling effect (rapid water evaporation), or change in physical state from a semisolid to a lower viscosity liquid. In the case of the Refreshing Gel Cream, a cream gel to liquid phase transition is the sensorial cue. It should be noted that shearing between two plates does not instigate the cream to liquid transition—factors from the skin surface appear critical to the perceived spreading rheology.

The initial perception of the Buttery Cream is that it has discernible viscous resistance. It is very matte, indicating that it has a dry feel. It does, however, start to thin with continued rubbing and thinning of the film, which is a gradual process and not noted as an abrupt collapse of structure. As mentioned below, this is probably why the Buttery Cream is ranked fairly low on quick break. It has a viscous characteristic during rubbing, which is distinct from the Refreshing Gel Cream (lighter feel) and Sunscreen Gel SPF-50 (the lightest feel). The Buttery Cream is a wax-based structure, therefore, there is no sustained cushion. Usually waxy structures require greater preliminary forces to break down the structure, but then they transition quickly to a fluid—especially if melting transitions are encountered. This phenomenon is clearly evident if one examines the Lissajous plot shown in Figure 4C, which undergoes a more drastic shape change than the other products examined. As with the Refreshing Cream, the skin surface environment conspicuously impacts the rheological outcome.

The Cushion Cream is best characterized as slightly elastic with some pickup when the index finger is forced downward on the product and then retracted. It maintains its shape when placed on the skin, thereby illustrating its robust microstructure. It is a thick treatment with more flow-resistance characteristics than the other samples. The initial feel characteristics reveal a large viscous component as the product thins, while during the secondary and final rub-in, a powder-like texture is experienced. There is no quick break, and the product absorbs into the skin rather quickly. Also, there is no tack, and the rich formula remains very dry throughout the sensorial test. The texture of the Cushion Cream is based on a hybrid polymer and wax structure; however, the polymer is the dominant structuring agent. In general, cushion is related to elasticity and flexibility, properties common in polymers. Waxes, on the other hand, are crystalline, less tough, and require greater initial forces to manipulate form.

Comparing the sensorial and rheology data, we can make several conclusions about the relationship between these two data sets. The mean quick break sensorial data ranks as follows: Refreshing Gel Cream (5.4 ± 0.6) > Sunscreen Gel SPF-50 (2.4 ± 0.9) > Buttery Cream (1.3 ± 0.5) = Cushion Cream SPF-15 (1.3 ± 0.5). As already mentioned, quick break is a parameter related to the early perception of a change in structure. As judged by τ_0, ZSV, σ'_{max}, and the trends in Figures 5 and 9, the Sunscreen Gel SPF-50 has the softest microstructure. The soft microstructure potentially masks dramatic changes as the sample is spread onto the skin. The Refreshing Cream, on the other hand, has a rather cohesive structure, even though it is softer than the Buttery Cream and Cushion Cream SPF-15; however, the Refreshing Gel Cream is sensitive to the chemistry of the skin surface and appears to melt when sheared. The transition from a cohesive soft solid to flow is

dramatic. No difference in quick break is seen between the Cushion Cream SPF-15 and Buttery Cream, where both prototypes are sampled with the finger and, hence, warming of the Buttery Cream occurs before and during spreading. In the Lissajous curves, the Refreshing Gel Cream and Buttery Cream own the only significant changes in slope between 25° and 32°C with salt data (Figure 13)—where the slope of the Lissajous is proportional to a net decrease in the complex viscosity (η*). The Buttery Cream shows a dramatic change in overall stress, which affects other sensorial attributes, but the change may be very rapid and closely related to how the sample is delivered to the skin; or, the gradual melting, although ultimately dramatic, is not seen as a quick break. Nevertheless, the change in viscosity is clearly evident after rubbing the Buttery Cream on the skin for a few seconds. The Cushion Cream SPF-15 formulation is only slightly affected by the salt and warmer temperature, and no evidence of a quick break is noted. The Sunscreen Gel SPF-50 exhibited a slight break—this change cannot be clearly discerned by the Lissajous plot and could be more related to how the sample microstructure is initially sheared when delivered to the skin (via a pump chassis).

Trends in perceived slip versus LAOS are as follows: Sunscreen Gel SPF-50 (7.6 ± 1.3) > Refreshing Gel Cream (6.6 ± 0.5) > Buttery Cream (4.8 ± 0.5) > Cushion Cream SPF-15 (4.6 ± 0.9). The σ_{max} (ambient temperature, smooth, no salt) displays a significant link ($R^2 = 0.992$) with the panel data, suggesting that the summation of viscous and residual elastic stress after shearing correlates with perceivable slip. Interestingly, but not surprisingly, the slip panel data also correlate well with stress data from low shear rate Lissajous analyses ($R^2 = 0.905$; Figure 9). The correlation no doubt includes the manifestation of wall slip, which is a reality at lower shear rates for all four textures; hence, wall slip effects in rheometry may relate to components of initial feel and the perception of slip.

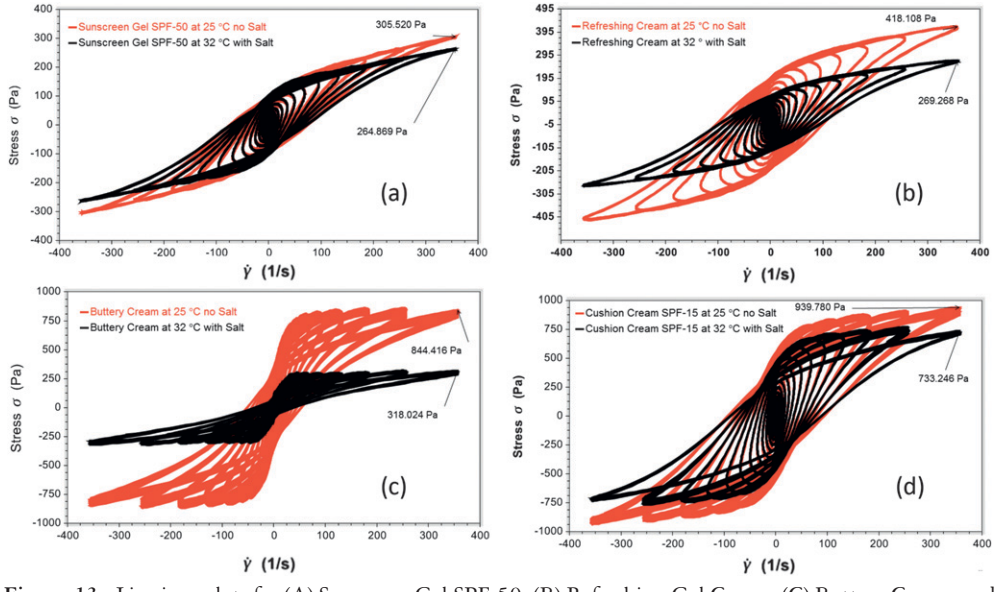

Figure 13. Lissajous plots for (A) Sunscreen Gel SPF-50, (B) Refreshing Gel Cream, (C) Buttery Cream, and (D) Cushion Cream SPF-15 with and without NaCl (500 nmol/cm^2). Systems tested at 25°C and no salt are meant to mimic the product in the jar, whereas testing at 32°C with electrolyte represents a model on-skin environment.

Cushion is ranked sensorially in the following order: Cushion Cream SPF-15 (6.4 ± 1.3) > Sunscreen Gel SPF-50 (5.2 ± 0.5) = Buttery Cream (5.2 ± 0.5) > Refreshing Gel Cream (3.6 ± 0.6). After removing Sunscreen Gel SPF-50 from the array of textures, it is evident that the cushion characteristic correlates with ZSV ($R^2 = 0.974$), and steady torsional with rough surfaces ($R^2 = 0.995$). From the LAOS data, the cushion data correlate well with the stress data at 32°C and salt ($R^2 = 0.958$), but less so with the 25°C no salt data ($R^2 = 0.783$). In low shear rate LAOS testing (maximum 4 s^{-1}) with no salt, the shapes of the Lissajous plots were very different, and so were the stress maxima. The stress maxima data correlated well ($R^2 = 0.994$) with the cushion data for Refreshing Gel Cream, Buttery Cream, and Cushion Cream SPF-15. In the final analysis, the TPA and rheology data did not correlate well with the expert panel's cushion data for the Sunscreen Gel SPF-50 formulation.

Light feel appears to be a more complex parameter as it is confounded by mid-to-late rub-out parameters; markers such as dry time, play time, and tribology could have an influence on the perceived texture. However, although correlation of ratings with LAOS and standard rheology was scattered, it appears that the impact of the formulation with the *in-vivo* skin environment influenced the light-feel ratings for the Refreshing Cream. More intriguing is the perception of the Cushion Cream SPF-15, which has a high resistance to spreading at first, but becomes powdery and dry as the emulsion breaks and components vaporize and wick into the stratum corneum. All said, the overall sensorial rating for light feel appears to point to perceived mid-to-late feel properties of the Cushion Cream SPF-15. Finally, the Sunscreen Gel SPF-50 and Buttery Cream are perceived as having the same light feel properties—evidently these are rated in the mid-to-late spreadability zone, after the Buttery Cream melts and interacts with skin surface electrolyte. The Sunscreen Gel SPF-50 is oily and has a long play time, giving ample time to rate its average resistance to spreading.

In summary, the sensorial data correlate with changes that are observed in the Lissajous plots as well as in the magnitudes of other rheological parameters. Rheological analyses, while very instructive for examining the perceived intensities of textures, do not allow differentiation in emotional or hedonic ratings, such as acceptability, color, odor, shine, cooling/warming, moistness, or matte effects; further, fine morphological properties of texture, including grittiness, smoothness, and graininess, are not well suited to rheological discrimination. Instead, rheology best correlates with the kinesthetic sensitivity of the muscles in the skin as the microstructure and/or viscosity of a product changes as a function of applied shear (23). Additionally, LAOS testing brings us much closer to the pictorial evaluation of a number of textural attributes that traditionally could only be monitored by expert panels, or estimated by a bevy of instrumental outcomes. For example, overlaying Lissajous plots of the four prototypes and qualitatively observing relative stress trends in the loop trajectories facilitate a cursory appraisal of textural properties, including cushion, spreadability, elasticity, stress dissipation, and viscosity (Figure 14). Ultimately, most traditional rheological data confer abstruse information about a single point in rheological time; in contrast, the Lissajous curve can be imagined as an unpretentious textural fingerprint that in one glance conveys a rheological snapshot of a formulation as its microstructure viscoelastically adapts to the influence of increasing shear strains.

NEXT STEPS: TRIBO-RHEOMETRY

Although outside the scope of this work, which focuses on correlating elastoviscoplastic rheological transitions, Kavehpour and McKinley (24) describe a novel triborheometry

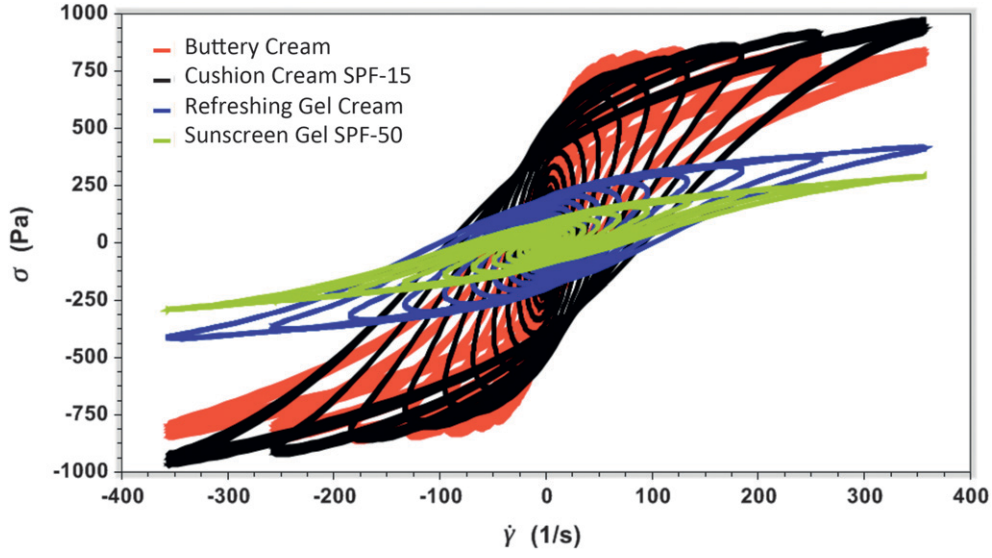

Figure 14. Lissajous curve overlay (25°C) for Sunscreen Gel SPF-50, Refreshing Gel Cream, Buttery Cream, and Cushion Cream SPF-15. The plot shows the similarity in total stress magnitude between the Buttery Cream and Cushion Cream SPF-15, where the Buttery Cream softens significantly at higher shear rates. The Refreshing Gel Cream and Sunscreen Gel SPF-50 scale similarly and are much softer, with the Refreshing Cream appearing slightly firmer than the Sunscreen Gel SPF-50. Complexities in flow, such as wall slip and plug flow, are comingled in the depicted instrumental stress response.

fixture to study complex fluids as they progress from viscometry (fluid) processes to tribology (friction) phenomena. When this tribo-rheometric geometry is affixed to a conventional rheometer, using large sample gaps produces measurements related to the bulk viscometric properties of the sample; however, as the gap is decreased to the order of the surface roughness of the plate (or attached substrate), the data becomes gap dependent and facilitates the calculation of friction coefficients between a fluid (e.g., cosmetic fluid) and a substrate (e.g., pig epidermis or Vitro-Skin®, IMS Inc., Portland, MA). Perhaps by coupling tribo-rheometry with LAOS methodology, and applying to very thin films along with the ability to control the chemistry, porosity, and topology of an affixed substrate, it may be possible to better comprehend, quantify, and visualize the transition from early rub-in (rheology) to after-feel (tribology) (24).

CONCLUSION

In this study, we outlined several novel techniques for the evaluation of formulation texture using nonlinear rheology (LAOS) to generate Lissajous plots, which serve as unique fingerprints for the rheological profile of each formulation. The Lissajous plots contain quantitative information, but, more importantly, they provide a visual interpretation of the rheological breakdown of the products as a function of shear, temperature, interfacial chemistry, and tribology. LAOS was specifically chosen to characterize formulation texture since its deformation and shear profiles most closely match the consumer experience *in vivo* during the rub-in application of skin-care products. While the LAOS data are indispensable for correlating to sensorial properties during rub-in of a cosmetic formula, we

also generated a significant amount of standard rheology data to better appreciate trends in Lissajous profiles, as well as to characterize the formulations with rheological parameters that more closely correspond to the initial tactile and at-rest properties of the formulation. Overall, our findings demonstrate that temperature, electrolyte, oscillatory shear rate, and the tribology/surface chemistry of the rheometer probes all impact the meaning of the data. Rough parallel plate surfaces challenge the integrity of the microstructure, while smooth data tend to better correlate with characteristics like slip. In addition to the complex rheology assessment, we also conducted TPA measurements to provide an overall characterization of key textural parameters of the formulation itself, such as firmness, cohesiveness, compressibility, resilience, etc. In several cases, comparison of these discrete attributes with results from linear and nonlinear rheology tests showed good correlation. Finally, sensorial analysis by an expert panel provided demonstrable discrimination between the distinct textural formulas and correlated well with several rheological parameters.

ACKNOWLEDGMENTS

We would like to thank the following individuals for their patience, cooperation, and important contributions to the article: Bharath Rajaram, Ph.D. (TA Instruments), Sarah Cotts, Ph.D. (TA Instruments), Professor Gareth H. McKinley, Ph.D. (MIT), William Thompson (Ashland, Inc.), Karine Deruddre (Ashland, Inc.), Nevine Issa (Ashland, Inc.), Diane Kennedy (Ashland, Inc.), Ritamarie Guerrero (Ashland, Inc.), James E. Brady, Ph.D. (Ashland, Inc.), Lexie Niemoeller, Ph.D. (TA Instruments), Alina Higham-Latshaw, Ph.D. (TA Instruments), Nathan Hesse, Ph.D. (TA Instruments), Aurelio Perez (TA Instruments), Tom Basalik (TA Instruments), David J. Moore, Ph.D. (GSK Consumer Healthcare), J.P. (writing partner and the world's most awesome 19 year-old feline), and Donald Koelmel (TRI-Princeton).

REFERENCES

(1) F. J. Pilgrim and D. R. Peryam, Quartermaster Food and Container Institute for the Armed Forces (U.S.) Food Acceptance Branch, *Sensory Testing Methods: A Manual*. (ASTM International, 1958).
(2) W. E. Craighead and C. B. Nemeroff, *The Concise Corsini Encyclopedia of Psychology and Behavioral Science*. (John Wiley & Sons, Hoboken, NJ, 2004), pp. 929–930.
(3) S. Guest, F. McGlone, A. Hopkinson, Z. Schendel, K. Blot, and G. Essick, Perceptual and sensory-functional consequences of skin care products, *J. Cosmet. Dermatol. Sci. App.,* **3,** 66–78 (2013).
(4) M. Bourne, "Food Texture," in *Encyclopedia of Agricultural, Food, and Biological Engineering*, D. R. Heldman, Ed. (Marcel-Dekker, New York, 2003), pp. 352–357.
(5) L. Gilbert, C. Picard, G. Savary, and M. Grisel, Impact of polymers on texture properties of cosmetic emulsions: A methodological approach, *J. Sensor. Stud.,* **27,** 392–402 (2012).
(6) M. Karsheva, S. Georgieva, and S. Alexandrova, Rheological behavior of sun protection compositions during formulation, *Kor. J. Chem. Eng.,* **29,** 1806–1811 (2012).
(7) T. Moravkova and P. Filip, The influence of thickeners on the rheological and sensory properties of cosmetic lotions, *Acta Polytech. Hung.,* **11,** 173–186 (2014).
(8) M. C. Taelman, J. C. Dederen, H. Peeters, and T. F. Tadros, Skin feeling quantification: An important formulators tool, *20th IFSCC Congress*, Cannes, France, September 14–18 (1998).
(9) E. K. Park and K. W. Song, Rheological evaluation of petroleum jelly as a base material in ointment and cream formulations: Steady shear flow behavior, *Arch. Pharm. Res.,* **33,** 141–50 (2010).
(10) R. E. Greenaway, *Psychorheology of Skin Cream*, Ph.D. Thesis, University of Nottingham, Nottingham, England (2010).

(11) L. Gilbert, G. Savary, M. Grisel, and C. Picard, Predicting sensory texture properties of cosmetic emulsions by physical measurements, *Chemometr. Intell. Lab.,* **124,** 24–31 (2013).
(12) S. Ozkan, T. W. Gillece, L. Senak, and D. J. Moore, Characterization of yield stress and slip behaviour of skin/hair care gels using steady flow and LAOS measurements and their correlation with sensorial attributes, *Int. J. Cosmet. Sci.,* **34,** 193–201 (2012).
(13) U. Yilmazer, and D. Kalyon, Slip effects in capillary and parallel disc torsional flows of highly filled suspensions, *J. Rheol.,* **33,** 1197–1212 (1989).
(14) R. Buscal, Wall slip in dispersion rheology, *J. Rheol.,* **54,** 1177–1183 (2010).
(15) A. Bot, I. A. van Amerongen, R. D. Groot, N. L. Hoekstra, and W. G. M. Agterof, Large deformation rheology of gelatin gels, *Polym. Gels Netw.,* **4,** 189–227 (1996).
(16) R. H. Ewoldt, A. E. Hosoi, and G. H. McKinley, New measures for characterizing nonlinear viscoelasticity in large amplitude oscillatory shear, *J. Rheol.,* **52,** 1427–1458 (2008).
(17) D. M. Kalyon, Shear viscosity and wall slip behavior of a viscoplastic hydrogel, *J. Rheol.,* **58,** 513–535 (2014).
(18) R. A. Freitas Jr., *Nanomedicine, Volume I: Basic Capabilities*. (Landes Bioscience, Georgetown, TX, 1999).
(19) D. J. Panther, and S. E. Jacob, The importance of acidification in atopic eczema: An underexplored avenue for treatment, *J. Clin. Med.,* **5,** 970–978 (2015).
(20) N. Nakagawa, S. Sakai, M. Matsumoto, K. Yamada, M. Nagano, T. Yuki, Y. Sumida, and H. Uchiwa, Relationship between NMF (lactate and potassium) content and the physical properties of the stratum corneum in healthy subjects, *J. Invest. Dermatol.,* **122,** 755–763 (2004).
(21) R. H. Ewoldt, P. Winter, J. Maxey, and G. H. McKinley, Large amplitude oscillatory shear of pseudoplastic and elastoviscoplastic materials, *Rheol. Acta,* **49**(2)**,** 191–212 (2010).
(22) R. L. McMullen, M. Gorcea, and S. Chen, "Emulsions and Their Characterization by Texture Profile Analysis," in *Formulating Topical Applications—A Practical Guide*, *1st Ed*, N. Dayan, Ed. (Allured Books, Carol Stream, IL, 2013), pp. 131–153.
(23) M. C. Meilgaard, C. V. Civille, and B. T. Carr, *Sensory Evaluation Techniques, 4th Ed*. (CRC Press, Boca Raton, FL, 2007), pp. 7–24.
(24) H. P. Kavehpour and G. H. McKinley, Tribo-rheometry: From gap-dependent rheology to tribology, *Tribol. Lett.,* **17**(2)**,** 327–335 (2004).

APPENDIX 1

Table AI
Sunscreen Gel SPF-50

Ingredients			
Trade name	INCI name	% w/w	Supplier
Phase A			
Escalol™ 517 UV filter	Butyl methoxydibenzoylmethane	3	Ashland
Escalol™ S UV filter	Bis-ethylhexyloxyphenol methoxyphenyl triazine	2	Ashland
Escalol™ 587 UV filter	Ethylhexyl salicylate	5	Ashland
Escalol™ HMS UV filter	Homosalate	10	Ashland
Escalol™ 597 UV filter	Octocrylene	8	Ashland
X-Tend™ 226 ester	Phenethyl benzoate	3	Ashland
Phase B			
Ceraphyl™ 31 ester	Lauryl lactate (and) myristyl lactate (and) cetyl lactate	6.5	Ashland
Ceraphyl™ 230 ester	Diisopropyl adipate	7	Ashland
Ceraphyl™ ICA ester	Isocetyl alcohol	2.5	Ashland
Ceraphyl™ SLK ester	Isodecyl neopentanoate	1	Ashland
Jeechem® CTG	Caprylic/capric triglyceride	1	Jeen International
Pelemol® 89	Ethylhexyl isononanoate	4	Phoenix Chemical
Phase C			
Allianz™ OPT polymer	Acrylates/C12-22 alkyl methacrylate copolymer (and) water/Aqua (and) propylene glycol	1	Ashland
Phase D			
SD Alcohol 40 B 200	Alcohol	41.79	-
FlexiThix™ polymer	PVP	4	Ashland
FD&C Blue 1 (Sol. 0.1%)	Water/aqua (and) CI 42090 (blue 1)	0.16	-
D&C Green 5 (Sol. 0.1%)	Water/aqua (and) CI 61570 (green 5)	0.05	-
Total		100	

Table AII
Refreshing Gel Cream

Ingredients			
Trade name	INCI name	% w/w	Supplier
Phase A			
Purified Water	Water/aqua	QS	-
EDTA tetrasodium salt	Tetrasodium EDTA	0.05	Fisher
Phase B			
PolySurf™ 67 CS HMHEC	Cetyl hydroxyethylcellulose	0.1	Ashland
Phase C			
UltraThix™ P-100 polymer	Acrylic acid/VP crosspolymer	0.8	Ashland
Phase D			
Lubrajel™ Oil Free hydrogel	Water/aqua (and) glycerin (and) glyceryl acrylate/acrylic acid copolymer (and) PVM/MA copolymer	3	Ashland
Lubrajel™ II XD Free hydrogel	Water/aqua (and) glycerin (and) glyceryl polyacrylate	2	Ashland
Unicert Yellow 08005-J (sol. 0.1%)	Water/aqua (and) CI 19140 (yellow 5)	0.09	Sensient
Unicert Blue 05601-J (sol. 0.1%)	Water/aqua (and) CI 42090 (blue 1)	0.21	Sensient
Phase E			
Refined Shea Butter	Butyrospermum parkii (shea) butter	1.1	Ashland
Orchid Complex™ OS ester	Caprylic/capric triglyceride (and) cymbidium grandiflorum flower extract	3.5	Ashland
Phase F			
Surfin 96	Alcohol denat.	7	CristalCo
Belsil® DM 5	Dimethicone	4	Wacker
Phase G			
Purified Water	Water/aqua	1.5	-
Sodium Hydroxide	Sodium hydroxide	0.08	Fisher
Phase H			
GP4G SP™ biofunctional	Water/aqua (and) artemia extract	1	Ashland
PF Desiro Blue	Parfum/fragrance (and) limonene (and) linalool (and) citronellol (and) hydroxyisohexyl 3-cyclohexene carboxaldehyde	0.25	Luzi
Optiphen™ preservative	Phenoxyethanol (and) caprylyl Glycol	0.5	Ashland
Phase I			
Captivates™ HC5812 encapsulate	Water/aqua (and) mentha piperita (peppermint) oil (and) helianthus annuus (sunflower) seed oil (and) gelatin (and) acacia senegal gum (and) menthol (and) CI 77891 (titanium dioxide) (and) tocopheryl acetate (and) mica (and) potassium sorbate (and) potassium citrate (and) citric acid (and) CI 77288 (chromium oxide greens) (and) CI 77510 (ferric ferrocyanide) (and) CI 61565 (green 6)	2	Ashland
Total		100	

Table AIII
Cushion Cream SPF-15

Ingredients			
Trade name	INCI name	% w/w	Supplier
Phase A			
Purified Water	Water/aqua	QS	-
Lubrajel™ II XD free hydrogel	Water/aqua (and) glycerin (and) glyceryl polyacrylate	3	Ashland
Tetrasodium EDTA salt	Tetrasodium EDTA	0.03	Fisher
Phase B			
Belsil® DM10	Dimethicone	3	Wacker
Escalol™ 587 UV filter	Ethylhexyl salicylate (octisalate)	5	Ashland
Escalol™ 597 UV filter	Octocrylene	5	Ashland
Escalol™ S UV filter	Bis-ethylhexyloxyphenol Methoxyphenyl triazine	3	Ashland
Ceralution® H	Behenyl alcohol (and) glyceryl stearate (and) glyceryl stearate citrate (and) disodium ethylene dicocoamide PEG-15 disulfate	5	Sasol
Phase C			
Unipure white LC981 EM	CI 77891 (titanium dioxide)	2	Sensient
Phase D			
Purified Water	Water/aqua	25	-
FlexiThix™ polymer	PVP	1	Ashland
Phase E			
Optiphen™ Plus preservative	Phenoxyethanol (and) caprylyl glycol (and) sorbic acid	1.5	Ashland
Peptide Q10™ biofunctional	Water/aqua (and) propanediol (and) pentapeptide-34 trifluoroacetate	0.5	Ashland
Dub Diol	Methylpropanediol	3	Stearinerie Dubois
Zemea®	Propanediol	4	DuPont Tate & Lyle
Covacryl® MV 60	Sodium polyacrylate	1.5	Sensient
FD&C RED N°40 07700-C (sol.0.1%)	Water/aqua (and) CI 16035 (red 40)	0.8	Sensient
Unicert yellow 08005-J (sol.0.1%)	Water/aqua (and) CI 19140 (yellow 5)	1	Sensient
Phase F			
Acide Lactique (90%)	Lactic acid (and) water/aqua	0.15	Fisher
Phase G			
PF Soleil Rayonnant	Parfum/fragrance (and) benzyl salicylate	0.3	Technicoflor
Total		100	

Table AIV
Buttery Cream

Ingredients			
Trade name	INCI name	% w/w	Supplier
Phase A			
Purified water	Water/aqua	QS	-
Optiphen™ Plus preservative	Phenoxyethanol (and) caprylyl Glycol (and) sorbic acid	1.5	Ashland
Phase B			
Stabileze™ QM polymer	PVM/MA decadiene crosspolymer	0.15	Ashland
Phase C			
ProLipid™ 141 lamellar gel	Glyceryl stearate (and) behenyl alcohol (and) palmitic acid (and) stearic acid (and) lecithin (and) lauryl alcohol (and) myristyl alcohol (and) cetyl alcohol	5	Ashland
Ceraphyl™ 494 ester	Isocetyl stearate	4	Ashland
Ceraphyl™ SLK ester	Isodecyl neopentanoate	4	Ashland
Dow Corning® 580 Wax	Stearoxytrimethylsilane (and) stearyl alcohol	2	Dow Corning
Emulsynt™ GDL ester	Glyceryl dilaurate	3	Ashland
Phase D			
Gransil® DM-5	Dimethicone (and) polysilicone-11	3	Grant
Phase E			
Sodium Hydroxide	Sodium hydroxide	0.04	Acros
Purified water	Water/aqua	0.5	-
Phase F			
PF Bois Precieux	Parfum/fragrance	0.3	Technicoflor
Unipure Red LC 381 ADT-C	CI 77491 (iron oxides) (and) isopropyl titanium triisostearate (and) bis-hydroxyethoxypropyl dimethicone (and) PEG-2-soyamine (and) isophorone diisocyanate	0.03	Sensient
Phase G			
Purified water	Water/aqua	3	-
Elixiance™ biofunctional	Propanediol (and) water/aqua (and) schinus molle (leaf) extract	1	Ashland
Ronaflair® Balance Gold	CI 77891 (titanium dioxide) (and) mica (and) tin oxide	0.3	Merck
Covabead® Velvet 10	Polymethyl methacrylate	1	Sensient
Ronaflair® Balance Red	CI 77891 (titanium dioxide) (and) mica (and) tin oxide	1.2	Merck
Phase H			
Purified water	Water/aqua	15	-
Natrosol™ Plus 330 CS	Cetyl hydroxyethylcellulose	0.5	Ashland
Total		100	